DATA DRIVEN MAPPING AND ATTENUATION OF NEAR-SURFACE DIFFRACTORS

BY

Ayman Fazea Al-Lehyani

A Thesis Presented to the

DEANSHIP OF GRADUATE STUDIES

KING FAHD UNIVERSITY OF PETROLEUM & MINERALS

DHAHRAN, SAUDI ARABIA

In Partial Fulfillment of the
Requirements for the Degree of

MASTER OF SCIENCE

In

GEOPHYSICS

June, 2009

KING FAHD UNIVERSITY OF PETROLEUM AND MINERALS

DHAHRAN 31261, SAUDI ARABIA

DEANSHIP OF GRADUATE STUDIES

This thesis, written by **Ayman Fazea Al-Lehyani** under the direction of his thesis advisor and approved by his thesis committee, has been presented to and accepted by the Dean of Graduate Studies, in partial fulfillment of the requirements of the degree of MASTER OF SCIENCE IN GEOPHYSICS.

Thesis Committee

Dr. Abdullatif Al-Shuhail (Thesis Advisor)

Dr. Cesar Barajas-Olalde (Member)

Dr. Abdulaziz Al-Shaibani
Department Chairman

Dr. Gabor Korvin (Member)

Dr. Salam Adel Zummo
Dean of Graduate Studies

21/6/09

Date

To my beloved Parents, wife
and daughter

ACKNOWLEDGMENTS

Acknowledgment is due to the King Fahd University of Petroleum & Minerals for supporting this research and to Schlumberger for the financial sponsorship.

I wish to express my deep appreciation to Dr. Abdullatif Al-Shuhail who served as my major advisor for his continuous and valuable guidance and patient throughout the course of this research work. I also wish to thank my thesis committee member Dr. Cesar Barajas-Olalde from Schlumberger Dhahran Carbonate Research Center for his full support and the fruitful and valuable discussions and reviews. My thanks also go to my other thesis committee member Dr. Gabor Korvin for his valuable comments.

Special thanks are due to Dr. Wail Mousa from Schlumberger Dhahran Carbonate Research Center for his help and support. His valuable Matlab programming tips made this work much smoother. I also want to extend my gratitude to Mr. Khaled Nouh, Schlumberger Arabian Geomarket Manager, for his full support.

Also I will not forget my parents, my wife, my whole family and friends' prayers and support. To all of them I say thank you.

TABLE OF CONTENTS

LIST OF FIGURES ..... **VI**

ABSTRACT (ARABIC) ..... **IX**

ABSTRACT ..... **X**

INTRODUCTION **1**

1.1 INTRODUCTION 1
1.2 PROBLEM STATEMENT 3
1.3 LITERATURE REVIEW 4
1.4 OBJECTIVE 7

METHODOLOGY **8**

2.1 INTRODUCTION 8
2.2 MAPPING NEAR-SURFACE DIFFRACTORS 8
2.3 ATTENUATION OF NEAR- SURFACE DIFFRACTIONS 14

MODELING OF NEAR-SURFACE DIFFRACTORS **17**

3.1 INTRODUCTION 17
3.2 MODEL A: THREE DIFFRACTORS 19
3.3 MODEL B: THREE-CLUSTERS OF THREE DIFFRACTORS 23

RESULTS & DISCUSSION **29**

4.1 INTRODUCTION 29
4.2 MAPPING RESULTS 29
4.2.1 Model A *29*
4.2.2 Model B *39*
4.3 ATTENUATION RESULTS 54
4.3.1 Model A *54*
4.3.2 Model B *63*

CONCLUSIONS & RECOMMENDATIONS **73**

5.1 CONCLUSIONS 73
5.2 RECOMMENDATIONS 74

BIBLIOGRAPHY **75**

VITA **76**

LIST OF FIGURES

Figure 1-1: A cartoon showing a diffractor. The resulting diffraction hyperbola is clearly seen on the shot gather. *3*

Figure 1-2: Stacked seismic data, a) before removing scattered surface waves, and b) after removing scattered surface waves. We can see the big improvement in the continuity of reflectors after removing the scattered surface waves (from Herman and Perkins, 2006). *5*

Figure 2-1: Geometry used to calculate the time-offset relation of the side-scattered diffraction. *10*

Figure 2-2: Flowchart of Mapping Code. *13*

Figure 2-3: Flowchart of Attenuation Code. *16*

Figure 3- 1: Cartoon showing the angle ϕ *15*

Figure 3- 1: Cartoon showing the angle ϕ. *19*

Figure 3- 2: Plan view of the diffractor locations, the seismic source, and the 2 receivers lines in Model A. *20*

Figure 3- 3: Synthetic shot gather from Line-1 of Model A *21*

Figure 3- 4: Synthetic shot gather from Line-2 of Model A. *22*

Figure 3-5: Earth Model B showing five isotropic horizontal layers. *25*

Figure 3- 6: Plan view of the diffractor locations, the seismic source, and the two receive lines of Model B. *26*

Figure 3- 7: Synthetic shot gather from Line-1 of Model B showing the diffractions from the three diffractor clusters. *27*

Figure 3- 8: Synthetic shot gather from Line-2 of Model B showing the diffractions from the three diffractors clusters. *28*

Figure 4- 1: Semblance Map for Line-1 of Model A using surface wave velocity V=1050m/s. *31*

Figure 4- 2: Semblance Map for Line-1 of Model A using surface wave velocity V=1000m/s. *32*

Figure 4- 3: Semblance Map for Line-1 of Model A using surface wave velocity V=950m/s. *33*

Figure 4- 4: Semblance Map for Line-2 of Model A using surface wave velocity V=1050m/s. *34*

Figure 4- 5: Semblance Map for Line-2 of Model A using surface wave velocity V=1000m/s. *35*

Figure 4- 6: Semblance Map for Line-2 of Model A using surface wave velocity V=950m/s. *36*

Figure 4- 7: Semblance Map for Line-1 of Model A using surface wave velocity V=1000m/s (zoomed). *38*

Figure 4- 8: Semblance Map for Line-2 of Model A using surface wave velocity V=1000m/s (zoomed). *39*

Figure 4- 9: Semblance Map for Line-1 of Model B using surface wave velocity V=950m/s. *41*

Figure 4- 10: Semblance Map for Line-1 of Model B using surface wave velocity V=900m/s. *42*

Figure 4- 11: Semblance Map for Line-1 of Model B using surface wave velocity V=850m/s. *43*

Figure 4- 12: Semblance Map for Line-2 of Model B using surface wave velocity V=950m/s. *44*

Figure 4- 13: Semblance Map for Line-2 of Model B using surface wave velocity V=900m/s. *45*

Figure 4- 14: Semblance Map for Line-2 of Model B using surface wave velocity V=850m/s. *46*

Figure 4- 15: Semblance Map for Line-1 of Model B using surface waves velocity V=900m/s (zoomed on the common cluster a). *49*

Figure 4- 16: Semblance Map for Line-1 of Model B using surface wave velocity V=900m/s (zoomed on the common cluster b). *50*

Figure 4- 17: Semblance Map for Line-1 of Model B using surface wave velocity V=900m/s (zoomed on the common cluster c). *51*

Figure 4- 18: Semblance Map for Line-2 of Model B using surface wave velocity V=900m/s (zoomed on the common cluster a). *52*

Figure 4- 19: Semblance Map for Line-2 of Model B using surface wave velocity V=900m/s (zoomed on the common cluster b). *53*

Figure 4- 20: Semblance Map for Line-2 of Model B using surface wave velocity V=900m/s (zoomed on the common cluster c). *54*

Figure 4- 21: Synthetic shot gather from Line-1 of Model A. *56*

Figure 4- 22: Estimation of the three diffractions from Line-1 of Model A. 57

Figure 4- 23: Shot gather (Line-1 of Model A) after subtracting the estimated diffraction events. 58

Figure 4- 24: Synthetic shot gather from Line-2 of Model A. 59

Figure 4- 25: Estimation of the three diffractions from Line-2 of Model A. 60

Figure 4- 26: Shot gather (Line-2 of Model A) after subtracting the estimated diffraction events. 61

Figure 4- 27: Estimation of Ricker wavelet for trace no. 75 in the window of diffractor no. 3 in Line-1 Model A. 62

Figure 4- 28: Estimation of Ricker wavelet for trace no. 20 in the window of diffractor no. 3 in Line-1 Model A. 63

Figure 4- 29: Synthetic shot gather from Line-1 of Model B. 65

Figure 4- 30: Estimation of the three diffractions clusters from Line-1 of Model B, cluster (a) is picked as one diffractor, see Table 4- 4). 66

Figure 4-31: Shot gather (Line-1 of Model B) after subtracting the estimated diffraction events. 67

Figure 4-32: Synthetic shot gather from Line-2 of Model B. 68

Figure 4- 33: Estimation of the three diffractions clusters from Line-2 of Model B, cluster (a) is picked as one diffractor, see Table 4- 4). 69

Figure 4- 34: Shot gather (Line-2 of Model B) after subtracting the estimated diffraction events. 70

Figure 4- 35: Shot gather (Line-1 of Model B) after subtracting the estimated diffraction events using the true diffractors' locations. 71

Figure 4- 36: Shot gather (Line-2 of Model B) after subtracting the estimated diffraction events using the true diffractors' locations. 72

ملخص

المشتتات القريبة من سطح الأرض هي واحدة من المشاكل في طريقة الاستكشاف الزلزالية على اليابسة. تستطيع هذه المشتتات تشتيت طاقة الأمواج الزلزالية السطحية المنطلقة من المصدر الزلزالي فتلوث الإشارة الزلزالية المتلقاة عبر مستقبلات الإشارات الزلزالية –السماعات الأرضية. تظهر موجات الطاقة المشتتة من المشتتات القريبة من السطح بشكل قوي على السجلات الزلزالية المجمعة من مصدر واحد على هيئة قطع زائد –يسمى التشتت- مخفية الإشارة الزلزالية الضعيفة المنعكسة من باطن الأرض. يسبب هذا التشتت تعقيدات أكثر للعديد من طرق إزالة الأمواج الزلزالية السطحية من السجلات الزلزالية، لا سيما إذا كان المشتت بعيدا عن خط السماعات الأرضية. تمت تجربة طرق مختلفة للقضاء على التشتت من السجلات الزلزالية. من هذه الطرق على سبيل المثال، مصفوفات السماعات الأرضية، تقنيات التنقية ، و تقنيات معكوس تشتت موجات رايلي. كل من هذه الطرق لها قيود وعوائق. تقدم هذه الرسالة خوارزميات لمعالجة البيانات الزلزالية تقوم برسم مواقع المشتتات القريبة من السطح على الخريطة و إزالة تأثيراتها على السجلات الزلزالية المجمعة من مصدر واحد. تعتمد هذه الخوارزميات على حساب متوسط مربعات الخطأ و قياسات التماثل و الملاءمة المثلى لموجة ريكر. تم تطبيق الخوارزميات على بيانات مصطنعة من نموذجين أرضيين مبتكرين. يحتوي النموذج الأول على ثلاث مشتتات قريبة من سطح الأرض بينما يحتوي النموذج الثاني على ثلاث مجموعات من المشتتات. تحتوي كل مجموعة على ثلاث مشتتات متباعدة عن بعضها بمسافات مختلفة. أظهرت النتائج أن الخوارزميات عملت بشكلٍ ممتاز في معظم الحالات. واجهت الخوارزميات بعض المتاعب في حال أن المسافات الفاصلة بين المشتتات القريبة من السطح أقل من الطول الموجي للموجات السطحية.

ABSTRACT

Near-surface diffractors are one of the problems in land seismic exploration. They can scatter the surface wave energy emanating from the seismic source and contaminate the signal received by seismic receivers. The scattered energy from the near-surface diffractors manifests itself on seismic shot gathers as strong hyperbolic events, called diffractions, masking the weak reflected body waves. Diffractions present complications to most of surface waves suppression schemes, especially when they have been scattered by scatterers away from the line of receivers. Different methods have been tried to eliminate diffractions from seismic data e.g., geophone arrays, filtering, and inverse scattering of Rayleigh waves. Each of those methods has its own limitations. In this thesis processing algorithms to map near-surface diffractors of surface waves and attenuate their diffracted energy in seismic shot gathers are presented. The mapping algorithm is based on semblance measurement and time-offset relation while the attenuation algorithm is based on least mean square best-fit of Ricker wavelet. The algorithms have been applied on synthetic data from two different models. The first model has three near-surface diffractors while the second model has three clusters of near-surface diffractors. Each cluster consists of three near-surface diffractors, with distances between them varying form one cluster to another. The results of both algorithms were excellent in most of the cases. They only had problems when the separation between individual diffractors is below the expected wavelength of the surface wave.

CHAPTER 1

INTRODUCTION

1.1 Introduction

Driven by the growing demand for oil and gas the interest of the oil and gas companies has been shifted toward exploring more complex reservoirs and enhancing production from existing assets. This drift has introduced new challenges to the geoscientists and engineers in the industry. Delineating bypassed oil and gas, optimizing well placement and proactive monitoring of the reservoir fluid behavior over time are gaining more emphasis.

Because of those challenges, a better understanding of the reservoirs is needed. Hence, reliable high resolution data are required. Seismic imaging is a vital part in getting these data. The quality of seismic data is defined by the signal-to-noise ratio (SNR) and the frequency bandwidth of the signal – the wider the bandwidth the better the quality (Yilmaz, 1987). Over the years, geoscientists and engineers have tried to increase the seismic data quality by developing better acquisition survey designs and data processing algorithms.

One major cause of the poor seismic data quality is the effect of the near-surface region on the seismic wavefield. Most of the seismic processing techniques used to overcome this problem assume homogeneous, isotropic horizontally layered Earth. However, due to various physical and geological processes, the younger top layers near the Earth's surface can be complex and heterogeneous. Rough topography, sand dunes, karsts and glacial tills are the most common near-surface features that degrade the quality of seismic data.

The near-surface region can cause variation in travel times and amplitudes of upcoming reflections from deep targets. This effect of travel time variation is treated by different methods such as static corrections, surface-consistent deconvolution and re-datuming techniques.

Another effect of the near-surface complexities (which is the scope of this thesis) is the scattering of surface waves that can mask the reflections of interest. Sharp discontinuities in density due to geological features (for example karsts) or artificial objects buried in the near surface can act as a secondary source when they are encountered by surface waves (Figure 1-1). This study will focus on the surface waves scattering effect of near-surface heterogeneities, how it can be detected and eliminated.

This thesis is organized in five chapters. Chapter one gives a background about the problem and states the objective of the thesis. Chapter two describes the proposed methodology that has been followed in this thesis to solve the problem. Chapter three

introduces two models that have been built to test the method proposed to solve the problem. Chapter four presents the results of these tests. Finally, chapter five concludes with the main findings of the thesis and gives some recommendations for future work.

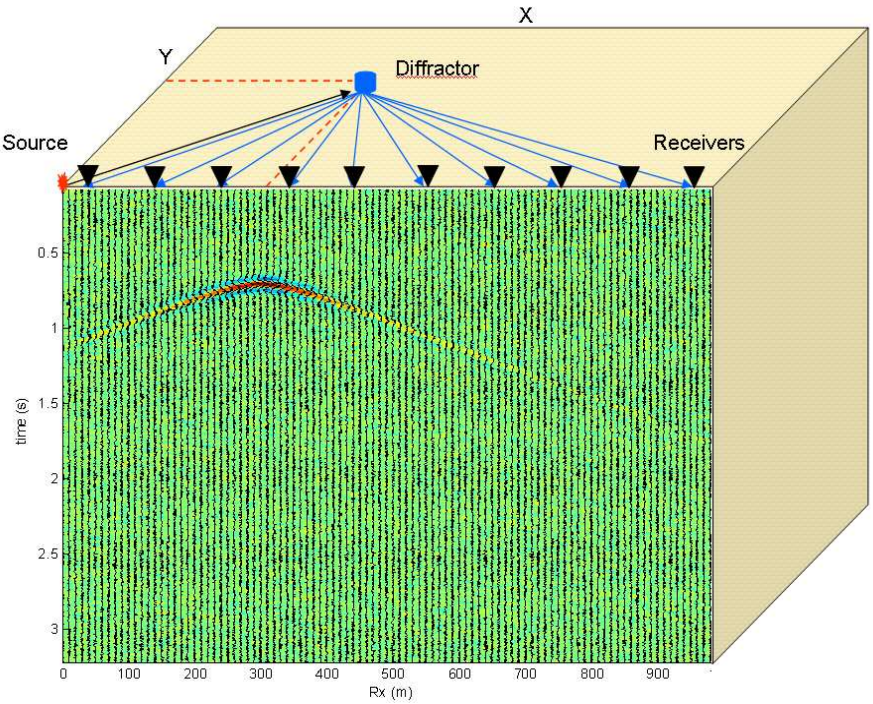

Figure 1-1: A cartoon showing a diffractor. The resulting diffraction hyperbola is clearly seen on the shot gather.

1.2 Problem Statement

Side-scattered surface waves from near-surface diffractors can mask the reflections coming from deep targets. In areas with severe near-surface complexities (sand dunes, karsts, wadis, etc.), removing scattered energy noise can be the key to have an

interpretable seismic image (Figure 1-2). Therefore, special processing algorithms are needed to solve the problem of scattered surface waves from near-surface diffractors.

1.3 Literature Review

Scattered surface waves from near-surface diffractors present a complication to most of the surface waves suppression schemes, especially when the waves have been scattered from scatterers away from the line of receivers. This last case refers to the so-called side-scattered waves. These kinds of waves are characterized by their low frequency, high amplitude and high hyperbolic moveout at near offsets**.** Different methods exist to reduce coherent scattered noise e.g., geophone arrays, filtering techniques, and wavefield-based techniques.

A common method to remove scattered surface waves is dip filtering in the frequency-wavenumber (f–k) domain (Yilmaz, 1987). Because near-surface side-scattered surface waves have partly hyperbolic moveout and hence high apparent velocities, their energy may lie in the pass zone of a dip filter, reducing its effectiveness to enhance the desired reflection energy.

Blonk and Herman (1994) derived an efficient model using inverse scattering of Rayleigh waves in a homogeneous elastic half-space, in which scatterers are distributed near the surface. With knowledge of the near-surface scattering distribution it is possible to calculate the scattered waves and subsequently subtract them from the data. An important step in this method is the correct estimation of the position of the sources generating the scattered waves.

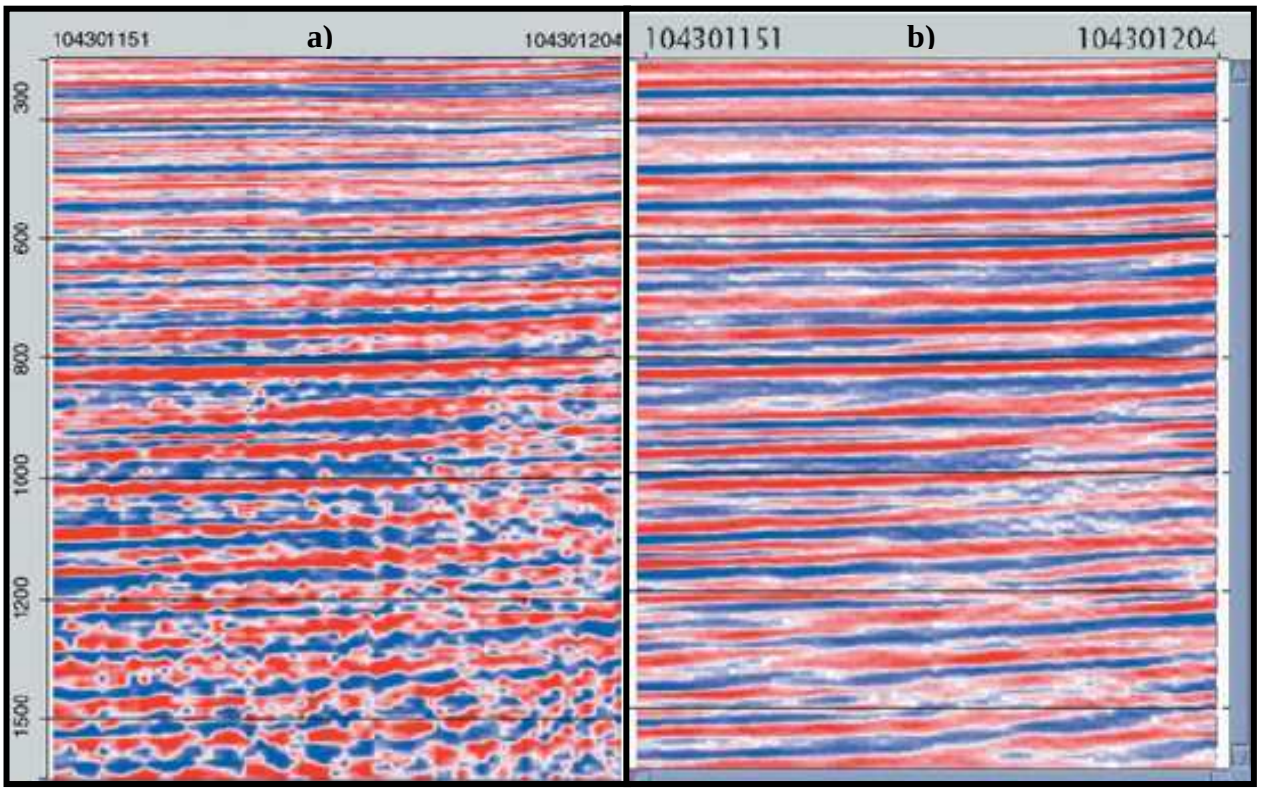

Figure 1-2: Stacked seismic data, a) before removing scattered surface waves, and b) after removing scattered surface waves. We can see the big improvement in the continuity of reflectors after removing the scattered surface waves (from Herman and Perkins, 2006).

Nemeth et al. (2000) proposed a method based on a new wavefield separation algorithm, called migration filtering, to address the scattering problem. In this method the wave-arrivals of the signal and the coherent noise are separated according to their travel path and their actual moveout characteristics.

During acquisition, properly chosen geophone arrays can suppress horizontally traveling surface waves through destructive interference which occurs when the signals from the geophones in the array are summed. However, to take care of the hyperbolic nature of the side-scattered noise, complex and large geophone-arrays are needed. This is a limitation as the trend in the industry now is moving toward the single geophone recording to eliminate the loss of high frequencies as a result of intra-array statics (Baeten et al., 2000). Al-Shuhail and Al-Ghamdi (2000) proposed a forward modeling method to locate and remove side-scattered noise from near-surface diffractors on land seismic shot gathers. They proposed a semblance analysis to scan for and locate the near-surface diffractors. Travel times for each located diffraction will be calculated and subtracted from the data.

Gulunay et al. (2006) proposed a similar method of locating and attenuating diffracted noise from heterogeneities in the water body of marine seismic surveys.

Following Blonk and Herman's (1994) method (i.e., predict-and-remove), Herman and Perkins (2006) derived a wavefield-based method to estimate and suppress near-surface side-scattered surface waves. Their method is based on a mathematical model whose parameters describe the essential properties of the scattered noise**.** After the parameters

are estimated; the noise is predicted and subtracted adaptively from the data. This technique is computationally extensive and complex. Therefore, to keep the method practical, a considerable number of approximations have to be made.

1.4 Objective

The objective of this thesis is to build a data driven processing algorithm to map near-surface diffractors of surface waves (in the x-y plane) and attenuate their diffracted energy in seismic shot gathers.

CHAPTER 2

METHODOLOGY

2.1 Introduction

The proposed method in this thesis is based on two main steps. The first step is to locate or map the near-surface diffractors on the x-y plane and identify their locations with respect to the seismic source and receivers using a seismic shot gather. The second step is to remove or eliminate their diffracted energy. This is done by modeling or estimating the diffracted energy using the seismic shot gather data as an input and then subtracting it from the seismic shot gather. This chapter explains these two steps in details.

2.2 Mapping Near-Surface Diffractors

To map diffractions (in the x-y plane) from the near-surface diffractors of surface waves in a seismic shot gather, an approach similar to that proposed by Al-Shuhail and Al-Ghamdi (2000) will be adopted. Based on the geometry of Figure 3, the side-scattering time-offset (T-X) relation from a near-surface diffractor can be represented by the following equation:

$$T(X) = (1/V)[\sqrt{(Dx - Sx)^2 + (Dy - Sy)^2 + (Dz - Sz)^2} + \sqrt{(Dx - Rx)^2 + (Dy - Ry)^2 + (Dz - Rz)^2}] \quad (2\text{-}1)$$

Where:

T(X) = Two-way travel time.

V= Velocity of surface waves.

Dx, Dy, Dz = x-, y-, z-Coordinates of the diffractor respectively.

Sx, Sy, Sz = x-, y-, z-Coordinates of the source respectively.

Rx, Ry, Rz = x-, y-, z-Coordinates of the receivers respectively.

In land seismic acquisition the geophones and sources can be laid on the surface so Rz and Sz can be taken as zero. Assuming that Dz ≈ 0 in the case of near-surface diffractors (surface waves that cause the scattering can hardly penetrate deeper than one wavelength) Equation 2-1 can be simplified to:

$$T(X) = (1/V)[\sqrt{(Dx - Sx)^2 + (Dy - Sy)^2} + \sqrt{(Dx - Rx)^2 + (Dy - Ry)^2}] \quad (2\text{-}2)$$

Based on Equation 2-2, we can calculate the travel time of the side-scattered energy of a near-surface diffractor at (Dx, Dy), on each receiver (Rx, Ry) generated by a surface wave traveling with a velocity V emanating from a seismic source at (Sx, Sy).

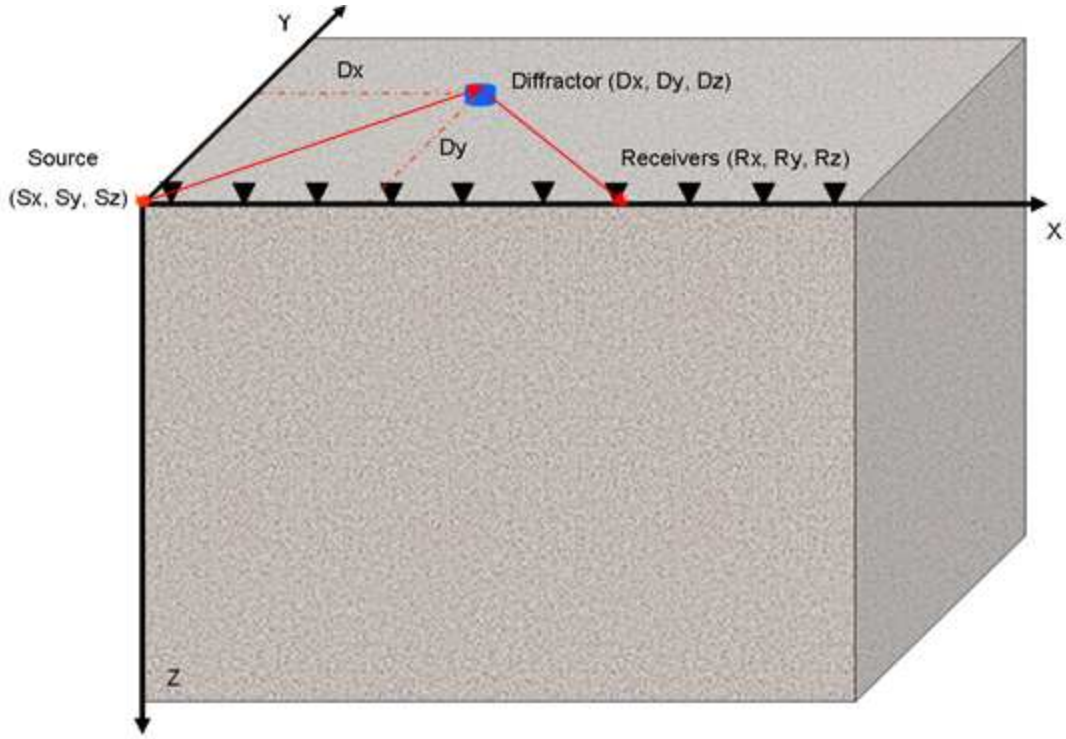

Figure 2-1: Geometry used to calculate the time-offset relation of the side-scattered diffraction.

To map diffractions (in the x-y plane) from the near-surface diffractors of surface waves in a seismic shot gather I developed a Mapping Code using MATLAB®. The Mapping Code grids an area around the receivers line (in the x-y plane) and assumes each point on that grid is a point diffractor and compute its corresponding hyperbolic travel time curve from Equation 2-2 using a specific surface wave velocity. Then to assess the assumption of a point on the grid being a diffractor, the semblance (Taner and Kohler,

1969) will be calculated in a window centered on the calculated diffraction travel time curve. The size of the window is equal to the surface wave dominant period.

So as an output, we will end up with a semblance value for each point on the grid, or in other words a Semblance Map. Points with high values on the Semblance Map are more likely to be diffractors. The user may try a range of surface waves velocities to generate multiple Semblance Maps. The Semblance Map corresponding to the velocity that is closest to the real velocity of surface waves will yield the highest semblance values (see Chapter 5).

The following steps –and the flow chart on Figure 4- summarize the Mapping Code algorithm:

1) Take as an input a seismic shot gather (in SEGY or SU format) and read all headers to obtain Sx, Sy, Rx, Ry, sampling rate (dt), record length in time (RL), etc.

2) Take as an input a range of expected velocities for the surface waves [Vmin – Vmax], velocity increment dV, and expected surface wave frequency fsw.

3) Starting with surface wave velocity V=Vmin, the code will calculate a set of diffractor locations {(Dx, Dy)} based on V and the record length (RL) such that $T(X) \leq RL$.

4) Calculate the T(X) using Equation 2-2 for each diffractor (Dx, Dy) using Vmin.

5) Compute the semblance from the shot gather in a window (equal to the dominant period of surface waves) around T(X) for each diffractor (Dx, Dy). That will give us a Semblance Map in the (x-y plane) for the velocity Vmin.

6) Increment V by dV and repeat steps (3)-(5) untill all velocities are exhausted.

7) Inspect Semblance Maps to determine probable diffractor locations and their associated surface-wave velocities.

8) Store {Dx,Dy,V} of each diffractor for later use by Attenuation Code.

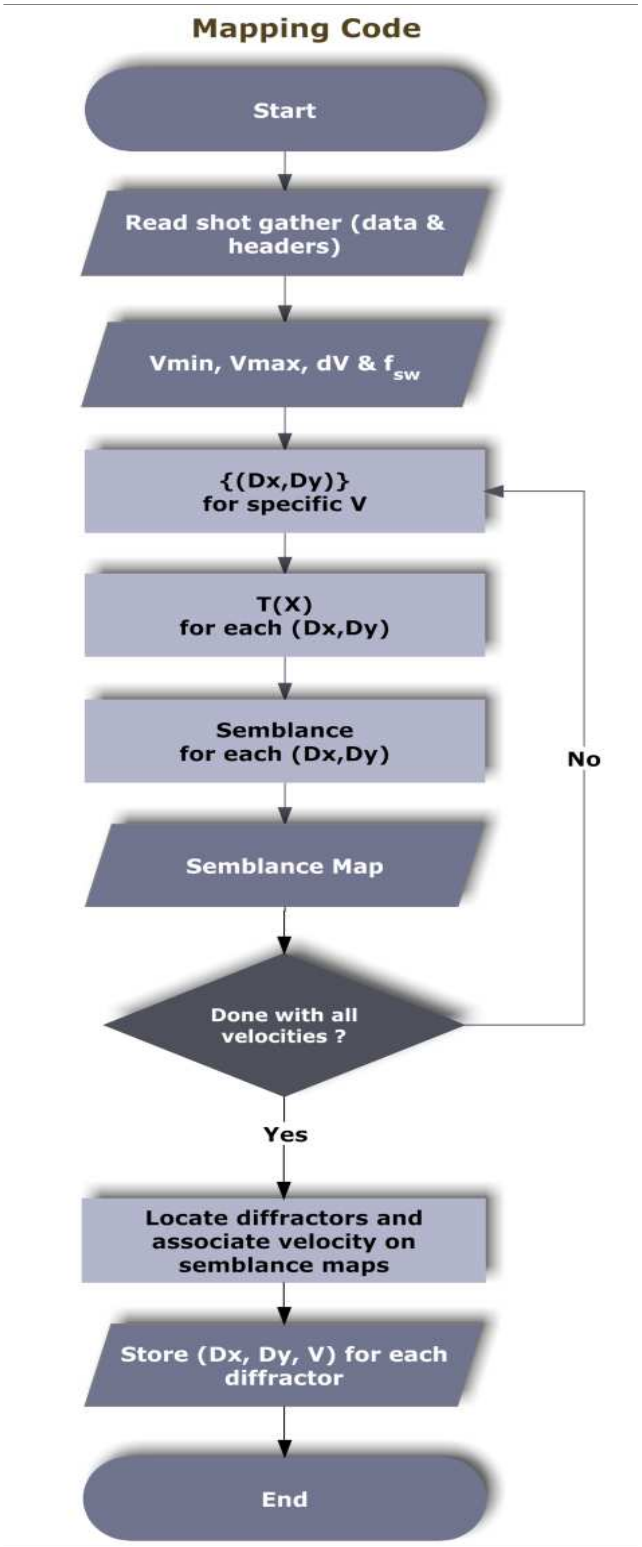

Figure 2-2: Flowchart of Mapping Code.

2.3 Attenuation of Near- Surface Diffractions

After identifying near-surface diffractor locations and their associated surface-wave velocities, the second part of this thesis work is to remove the near-surface diffractions from the seismic shot gather. Given diffractor locations {(Dx, Dy)} and their associated surface-wave velocities (V) I developed another MATLAB code to attenuate the near-surface diffractions (Attenuation Code).

The Attenuation Code calculates a diffraction hyperbola, using Equation (2-2), that corresponds to each {Dx,Dy,V} triplet using the coordinates of the source of the input shot gather {Sx,Sy} and all receivers along the input gather {Rx,Ry}. The code then selects all samples in a window centered around the calculated hyperbola. The size of the window equals the surface wave dominant period.

The next step is to estimate the diffracted signal s(t) in each window of each trace x(t) in the input shot gather. Each window of the trace x(t) is consisting of the diffracted signal s(t) and any other event (random noise, reflections, etc..) that we are considering as a noise n(t). The estimation of the diffracted signal Es(t) is accomplished by least-squares fitting of Ricker wavelets $s(t)=A*(1-2(\pi\ fsw\ t)\ 2)\ exp\ -(\ \pi\ fsw\ t)2$ (where A is the peak amplitude of the wavelet and fsw is it's frequency) to minimize the error e(t) between x(t) and s(t). Other types of wavelets can be used for fitting if the expected scattered wavelets

are considerably different from a Ricker wavelet (e.g., minimum-phase wavelets). The flow chart in Figure 5 summarizes the Attenuation Code algorithm.

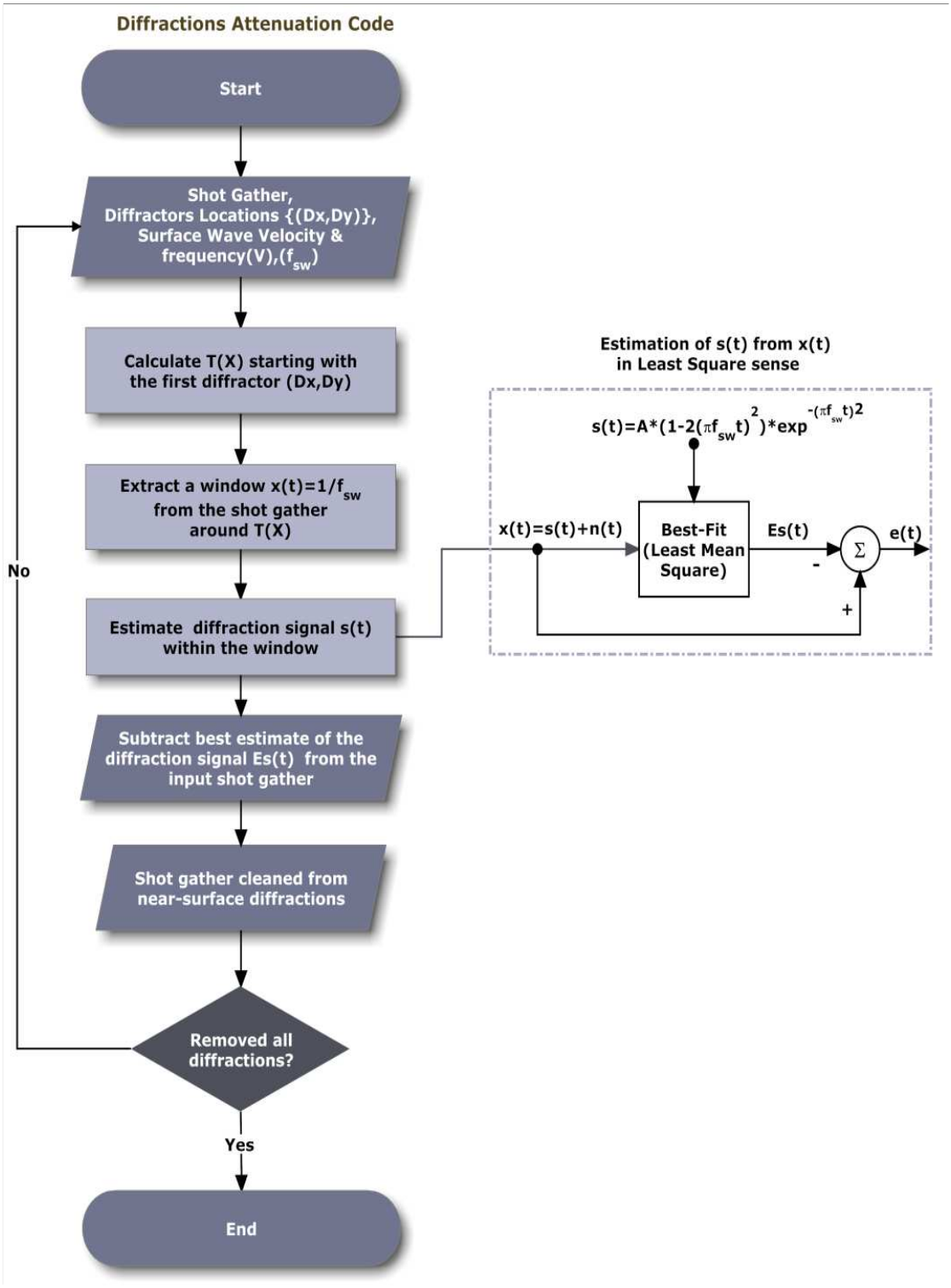

Figure 2-3: Flowchart of Attenuation Code.

CHAPTER 3

MODELING OF NEAR-SURFACE DIFFRACTORS

3.1 Introduction

Although the Mapping & Attenuation Codes work on single 2D shot gathers with one receiver line, the problem of near-surface diffractions is a 3D problem because the near-surface diffractors are located outside the receive line vertical plane . This is why I needed to develop my own 3D modeling code.

I developed a MATLAB modeling code (Diffraction Generation Code) to generate diffractions of surface waves from near-surface diffractors. I used Equation 2-2 to calculate the arrival times for each diffractor (Dx, Dy). Then I generated an empty seismic shot gather (all amplitudes on all traces are zeros) with a sampling rate $dt = 0.004$ s and I replaced the zero amplitudes at samples corresponding to the calculated diffractor arrival times with unit amplitude. After that I generated a Ricker wavelet using the following formula (Sheriff and Geldart, 1995):

$$w(t) = A\left(1 - 2(\pi \times fsw \times t)^2\right) \times e^{-(\pi \times fsw \times t)^2} \qquad (3\text{-}1)$$

.

I used a dominant frequency $fsw = 15$ Hz and amplitude $A = 1$ using the same sampling rate of $dt = 0.004$. Then, I convolved the Ricker wavelet with the seismic shot gather that has unit impulses at the diffractor travel times. Finally, I added an attenuation factor to the traces amplitude using a $Cos(\phi)$ factor (Yilmaz, 1987) where ϕ is the angle between the perpendicular line going from the diffractor point to the receiver line, and the straight line between the diffractor and the receiver (Figure 3-1).

Using the Diffraction Generation Code I generated four synthetic seismic shot gathers based on two different earth models (two shot gathers for each model). Those shot gathers will be used to evaluate my Mapping & Attenuation Codes (see Chapter 4).

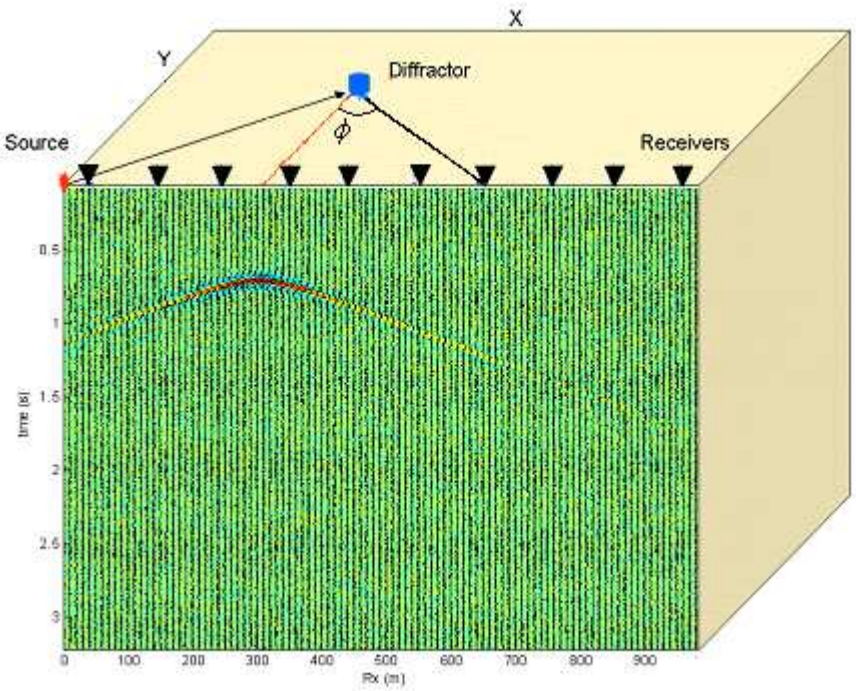

Figure 3- 1: Cartoon showing the angle ϕ.

3.2 Model A: Three Diffractors

This model consists of a simple homogeneous and isotropic half space. Using this model and my Diffraction Generation Code I added three near-surface diffractions at coordinates (300,0), (500,300) and (800,200) to two synthetic shot gathers, that I called Line-1 and Line-2, acquired on that model assuming a surface wave velocity V=1000 m/s. It should be noted here that the units of the x and y coordinates are meters. Each line consists of 101 receivers with a receiver spacing of 10 m. I also added 10% random noise with normal distribution (zero mean and 0.1 standard deviation) to the synthetic shot gathers. Figure 3-2 depicts a plan view of the diffractors' locations, the seismic source,

and the two receiver lines. Figures 3-3 & 3-4 depict both synthetic shot gathers (Line-1 and Line-2), respectively. The main purpose of this simple model was to test whether the Mapping and Attenuation Codes will be able to detect and attenuate these near-surface diffractions.

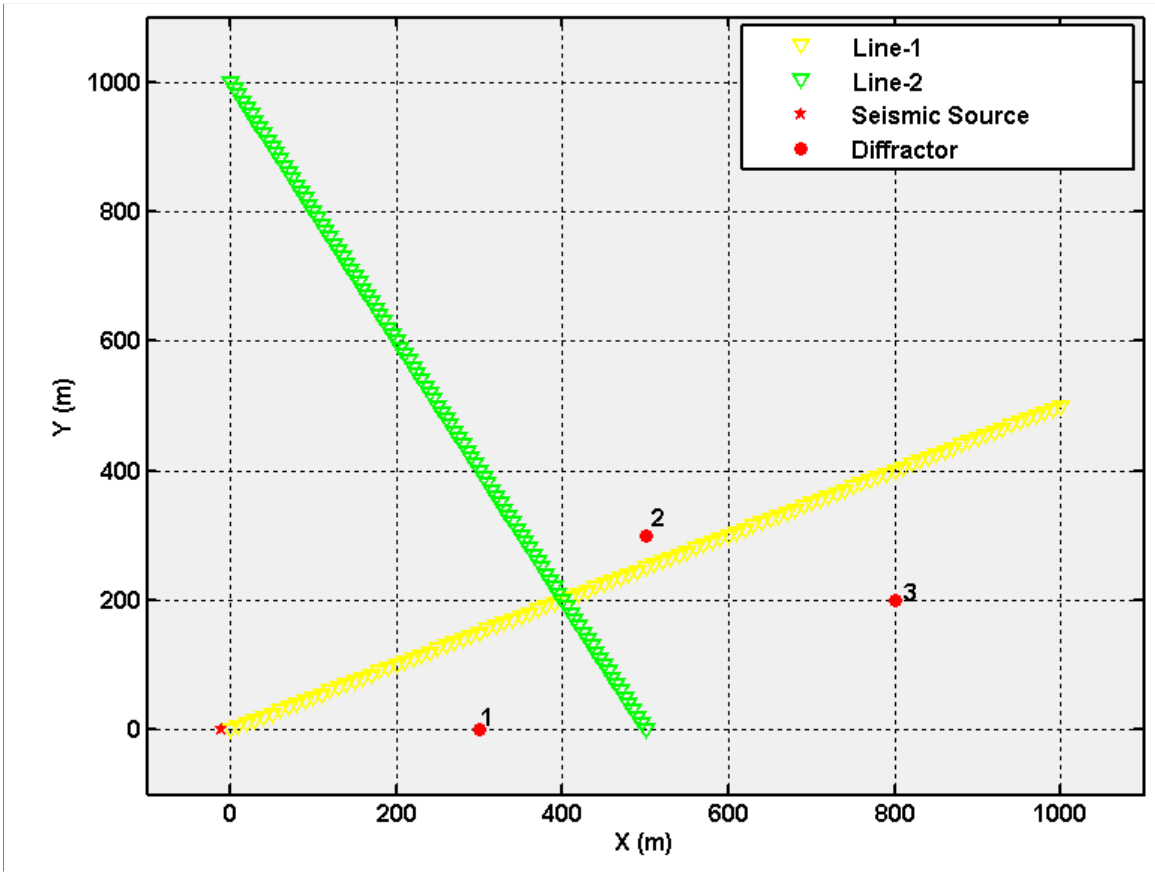

Figure 3- 2: Plan view of the diffractor locations, the seismic source, and the 2 receivers lines in Model A.

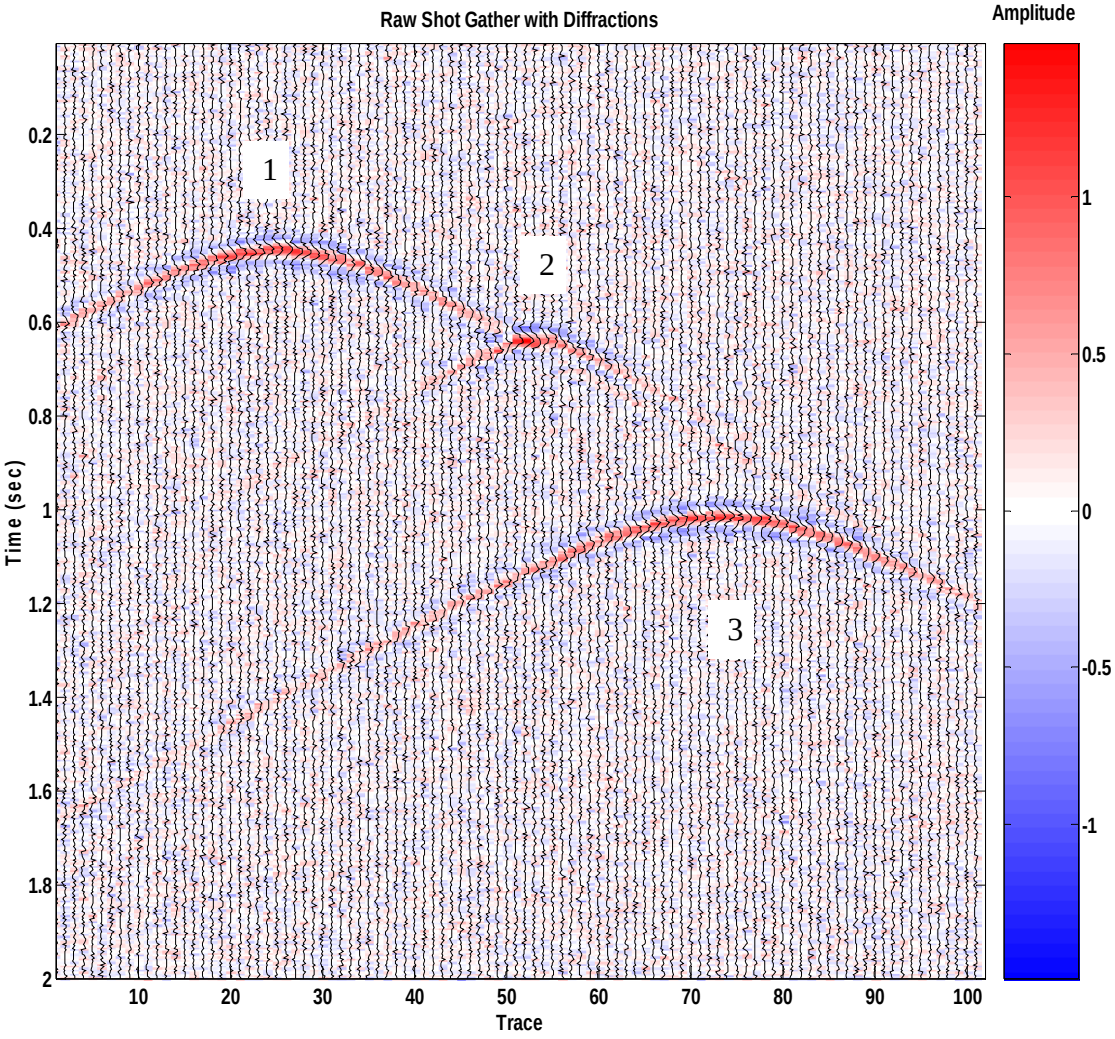

Figure 3- 3: Synthetic shot gather from Line-1 of Model A

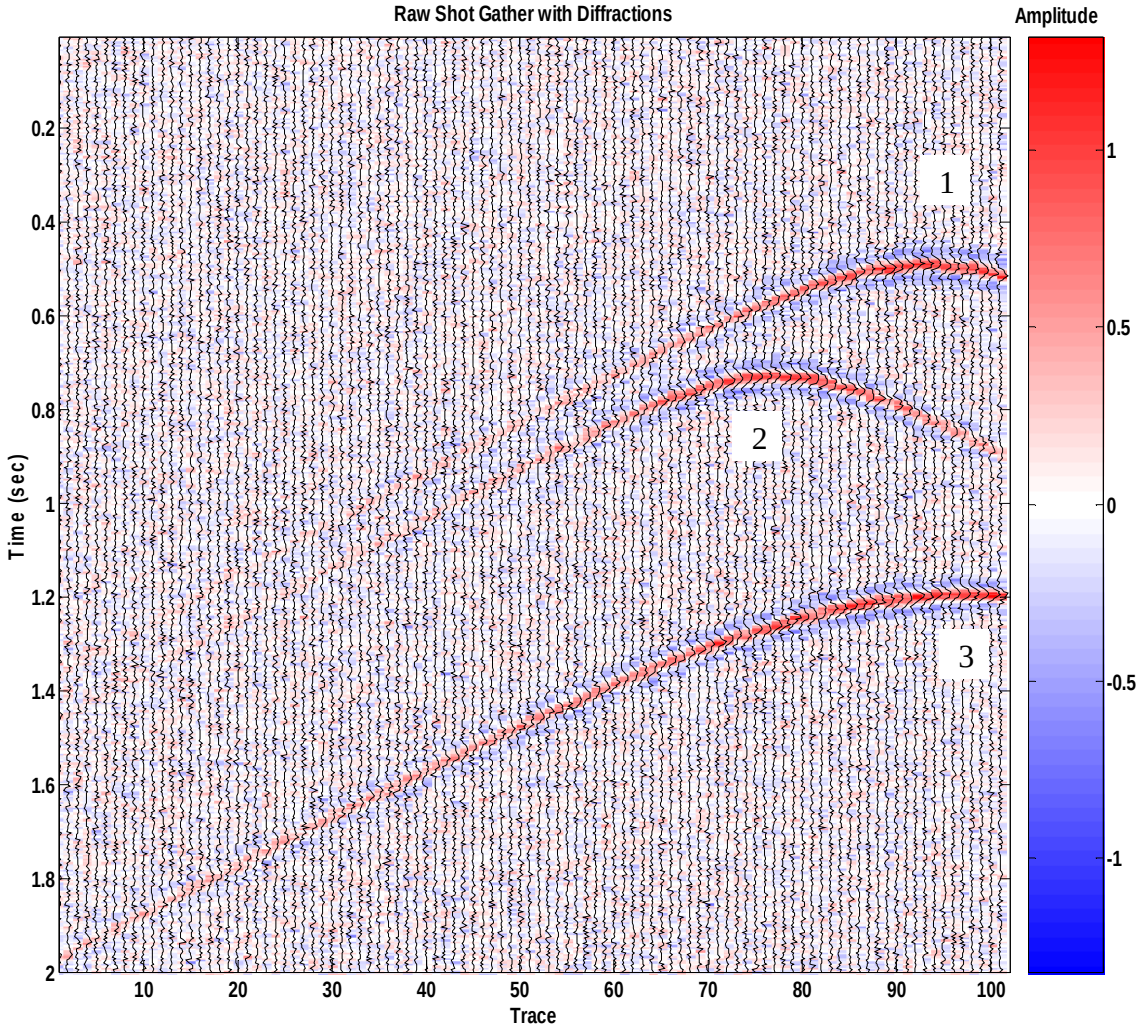

Figure 3- 4: Synthetic shot gather from Line-2 of Model A.

3.3 Model B: Three-Clusters of Three Diffractors

This model consists of five homogeneous, isotropic and horizontal layers with velocities (1800, 2300, 3800, 3400, 4200) m/s at depths of 0, 300, 900, 1,100 and 1,800 m, respectively (Figure 3-5). Using this model and my Diffraction Generation Code I added three clusters of near-surface diffractions to two synthetic shot gathers (Line-1 and Line-2) acquired on that model assuming a surface wave velocity V=900 m/s. Each cluster consists of three near-surface point diffractors, with distances between them varying form one cluster to another. Table 3-1 lists the locations of each diffractor in each cluster and the minimum and maximum distance between each cluster diffractors. Each Line consists of 201 receivers with a receiver spacing of 10 m. Figure 3-6 depicts a plan view of the diffractor locations, seismic source and the two receiver lines. Figure 3-7 and 3-8 are the synthetic shot gathers of Line-1 and Line-2, respectively with the three clusters of diffractions after adding 10% of normally distributed random noise. The main purpose of this model was to test the spatial resolution (the ability to differentiate between two closely spaced diffractors) of the Mapping Code and to test the ability of Diffractions Attenuation Code to attenuate closely spaced diffractions.

Cluster	Diffractor	Diffractor Location		Min. Distance Between Diffractors (m)	Max. Distance Between Diffractors (m)
		x (m)	y (m)		
a	1	150	200	10.00	22.36
	2	150	210		
	3	170	200		
b	1	800	50	25.00	101.12
	2	820	65		
	3	815	150		
c	1	1500	-500	111.80	206.16
	2	1550	-400		
	3	1600	-600		

Table 3-1: Locations of each diffractor in each cluster and the minimum and maximum distance within each cluster of diffractors.

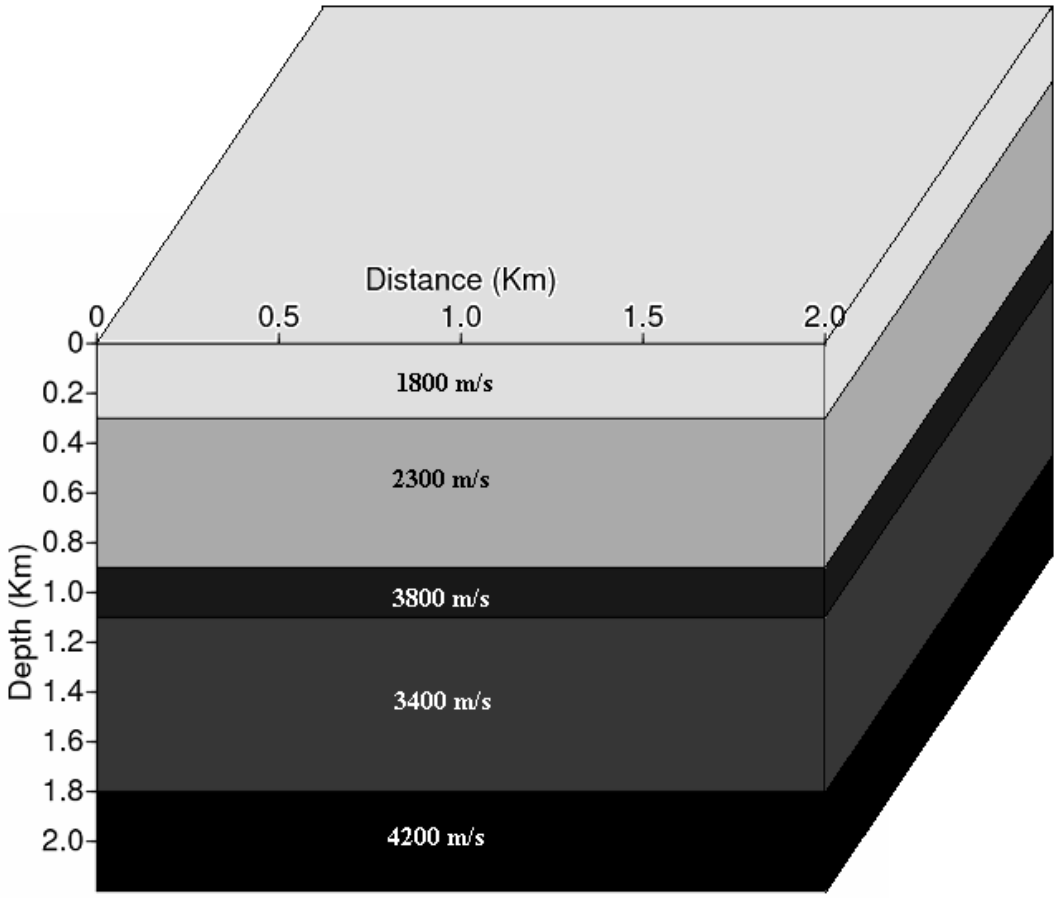

Figure 3-5: Earth Model B showing five isotropic horizontal layers.

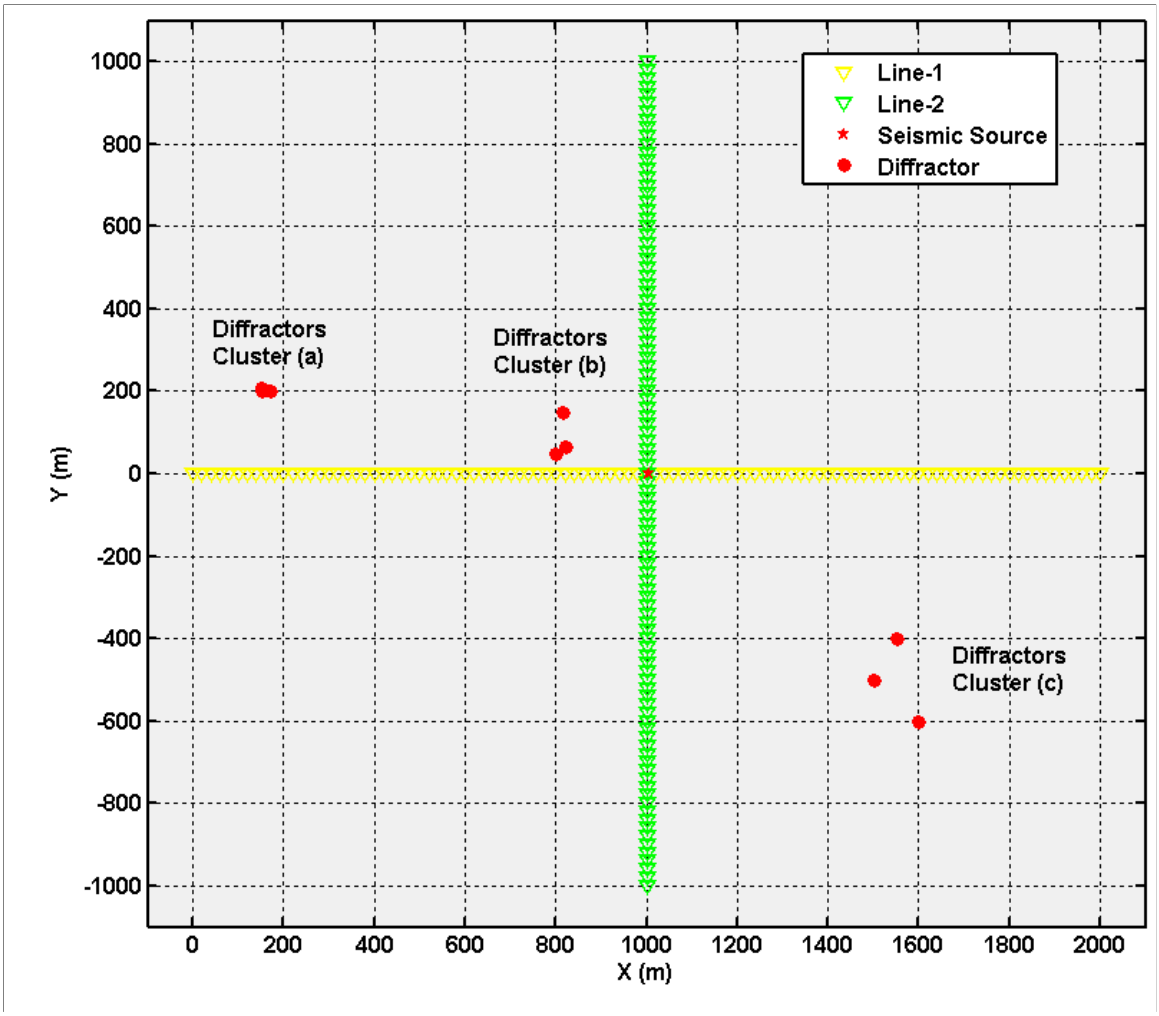

Figure 3- 6: Plan view of the diffractor locations, the seismic source, and the two receive lines of Model B.

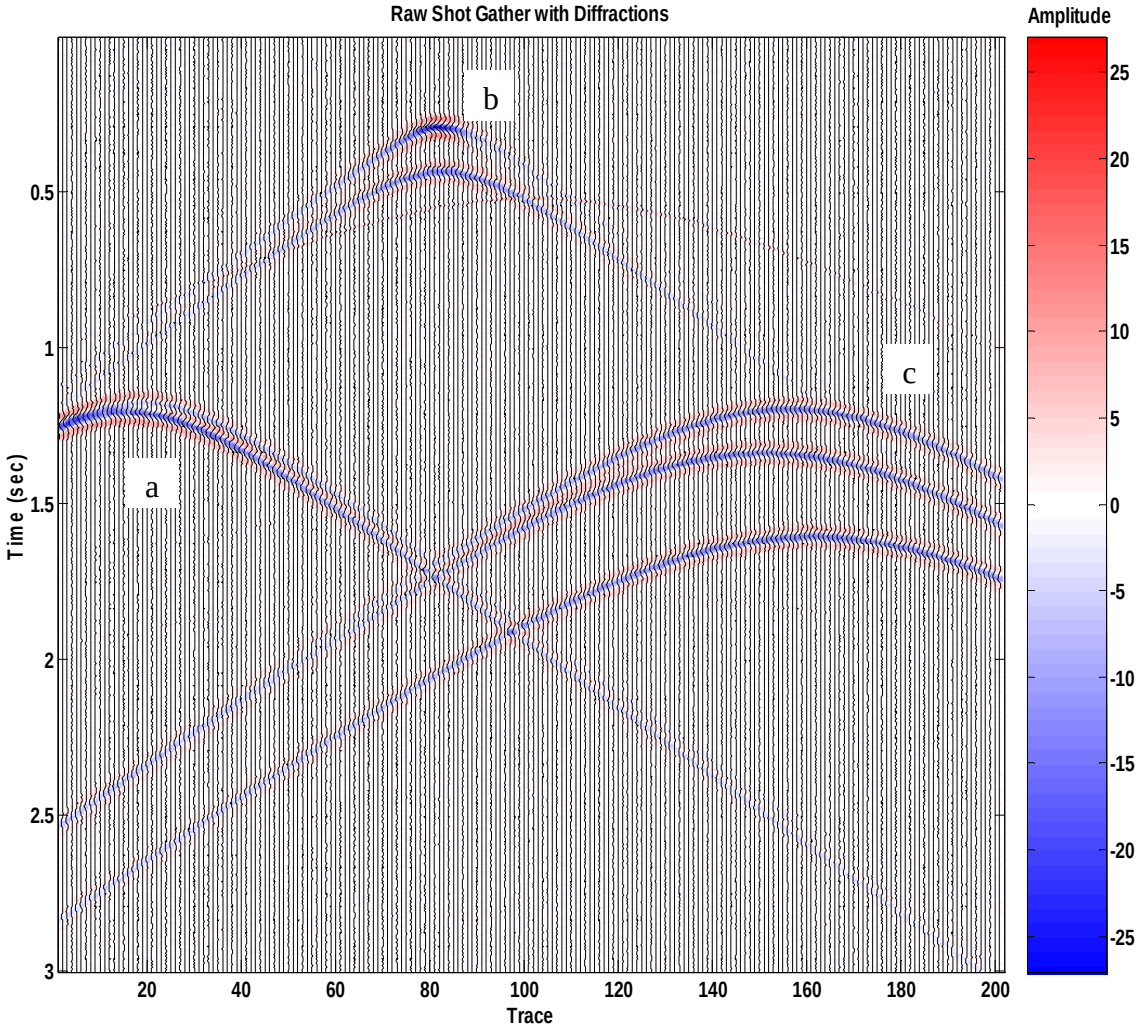

Figure 3- 7: Synthetic shot gather from Line-1 of Model B showing the diffractions from the three diffractor clusters.

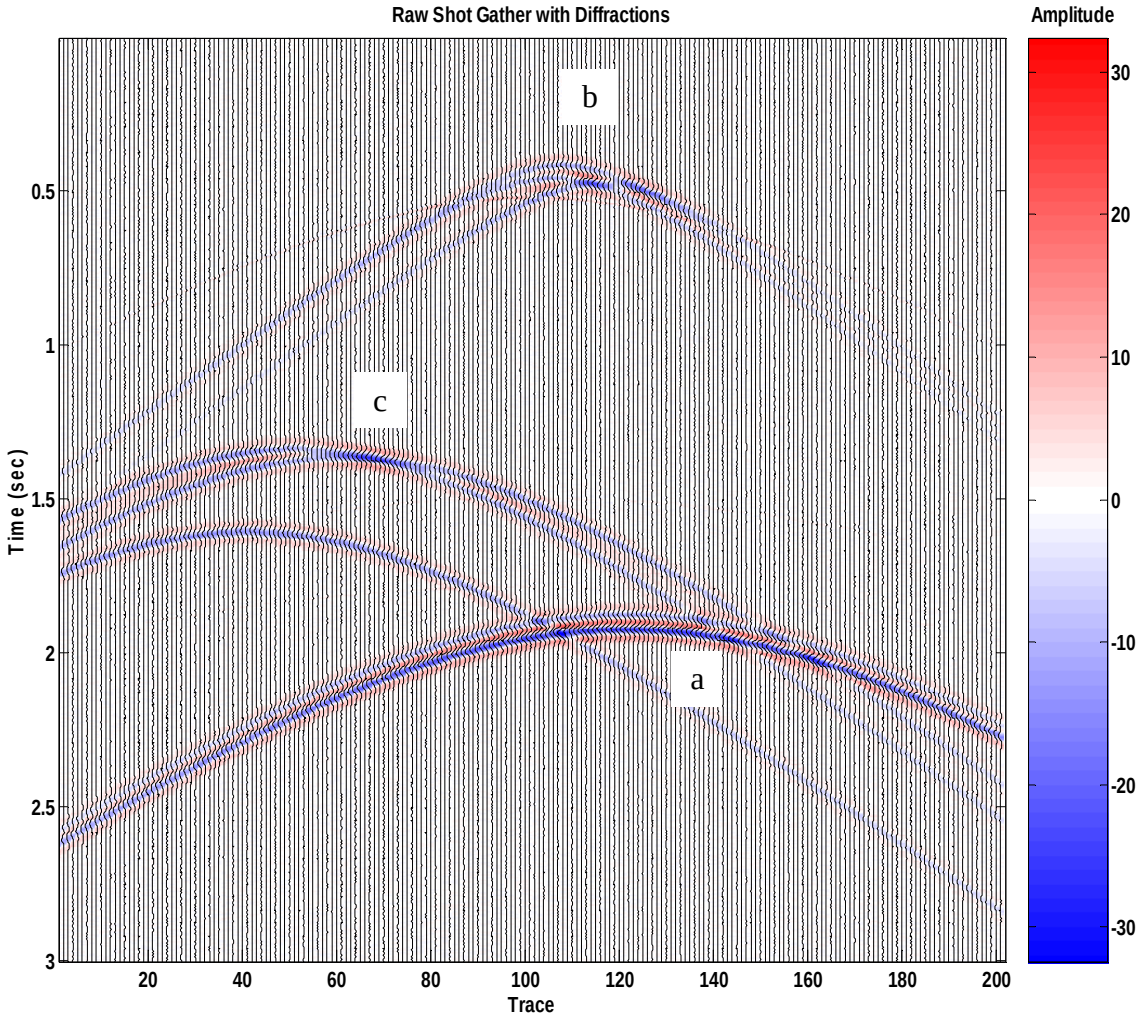

Figure 3- 8: Synthetic shot gather from Line-2 of Model B showing the diffractions from the three diffractors clusters.

CHAPTER 4

RESULTS & DISCUSSION

4.1 Introduction

The four synthetic seismic shot gathers from the two earth models A & B (introduced in Chapter 3) were used to test and evaluate the performance of the Mapping and Attenuation Codes. The Mapping Code is used to scan the shot gathers for possible near-surface diffractors, estimate their locations, and give the best estimate of surface wave velocity. The Attenuation Code is used to attenuate the associated diffractions events. This chapter summarizes the main results of these tests.

4.2 Mapping Results

4.2.1 Model A

The two synthetic seismic shot gathers (Line-1 and Line-2) from Earth Model A were used as input to the Mapping Code using three different velocities for surface waves, V=1050 m/s, V=1000 m/s (the true model velocity), and V=950 m/s with frequency

$fsw = 15Hz$. The Code generated three Semblance Maps for each shot gather, one for each velocity (Figures 4-1 to 4-6).

Table 4-1 summarizes the results of the six Semblance Maps. As expected, the best Semblance Maps for both shot gathers are the ones using the true velocity, V=1000 m/s (the ones with the highest semblance values, Figure 4-2 and Figure 4- 5).

Model A Semblance Maps summary				
Shot Gather	**Figure**	**Velocity (m/s)**	**fsw (Hz)**	**Maximum Semblance Value**
Line-1	**4-1**	**1050**	**15**	**0.28076**
	4-2	**1000**	**15**	**0.57154**
	4-3	**950**	**15**	**0.26491**
Line-2	**4-4**	**1050**	**15**	**0.44271**
	4-5	**1000**	**15**	**0.68797**
	4-6	**950**	**15**	**0.40648**

Table 4-1: Semblance Maps summary for Model A.

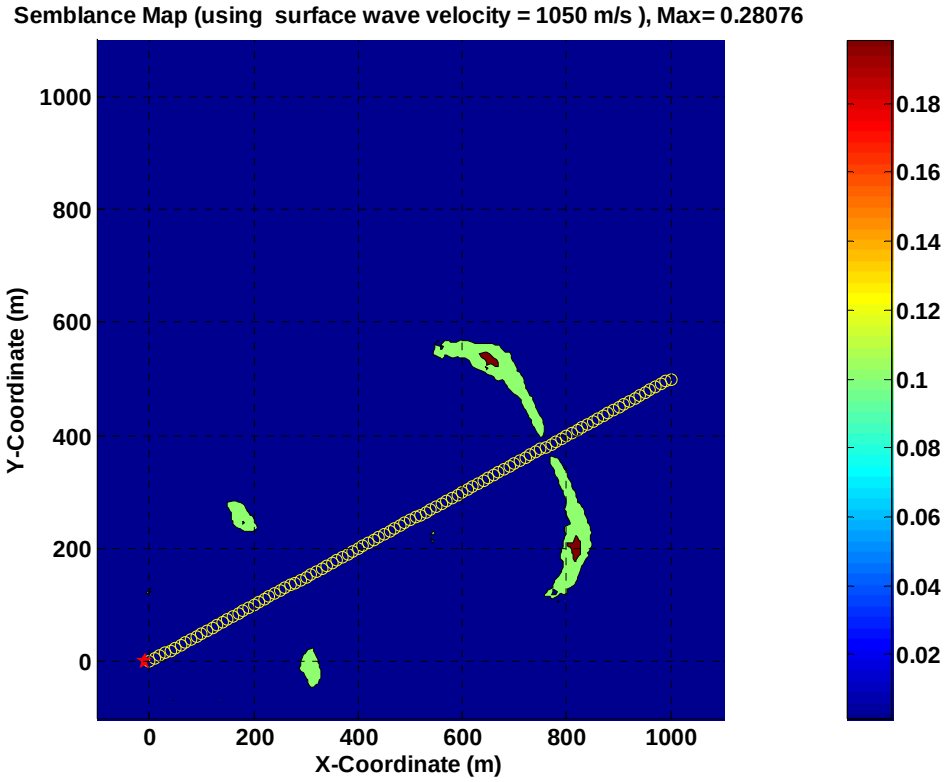

Figure 4- 1: Semblance Map for Line-1 of Model A using surface wave velocity V=1050 m/s.

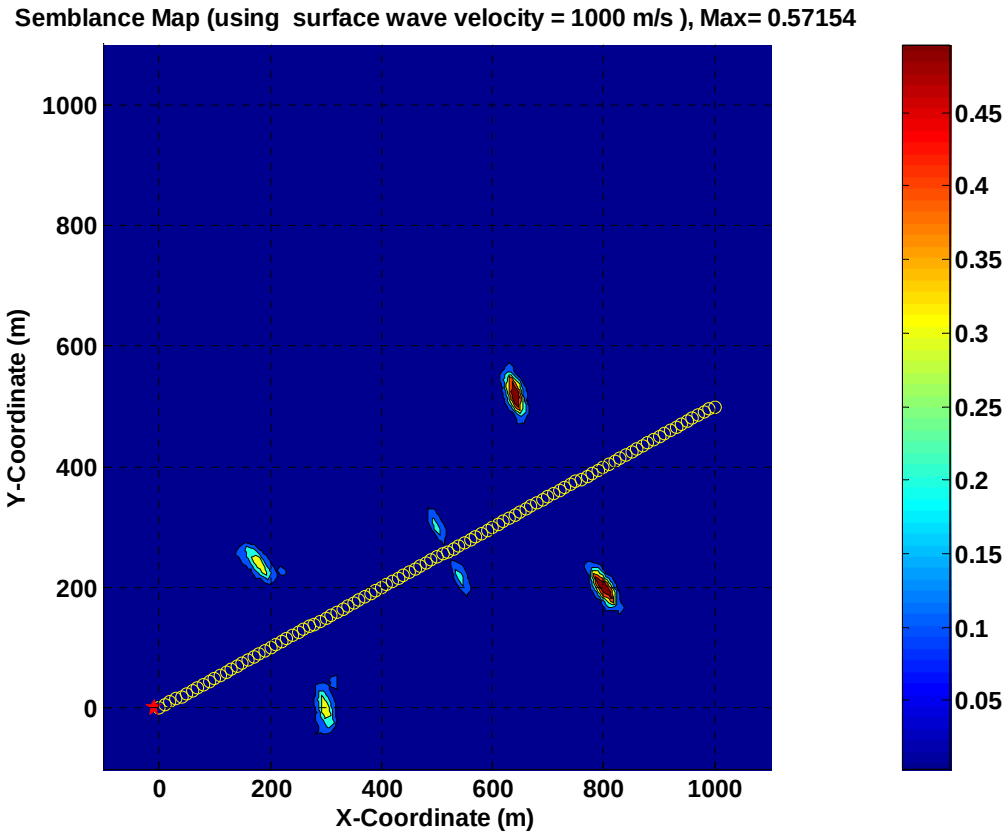

Figure 4- 2: Semblance Map for Line-1 of Model A using surface wave velocity V=1000 m/s.

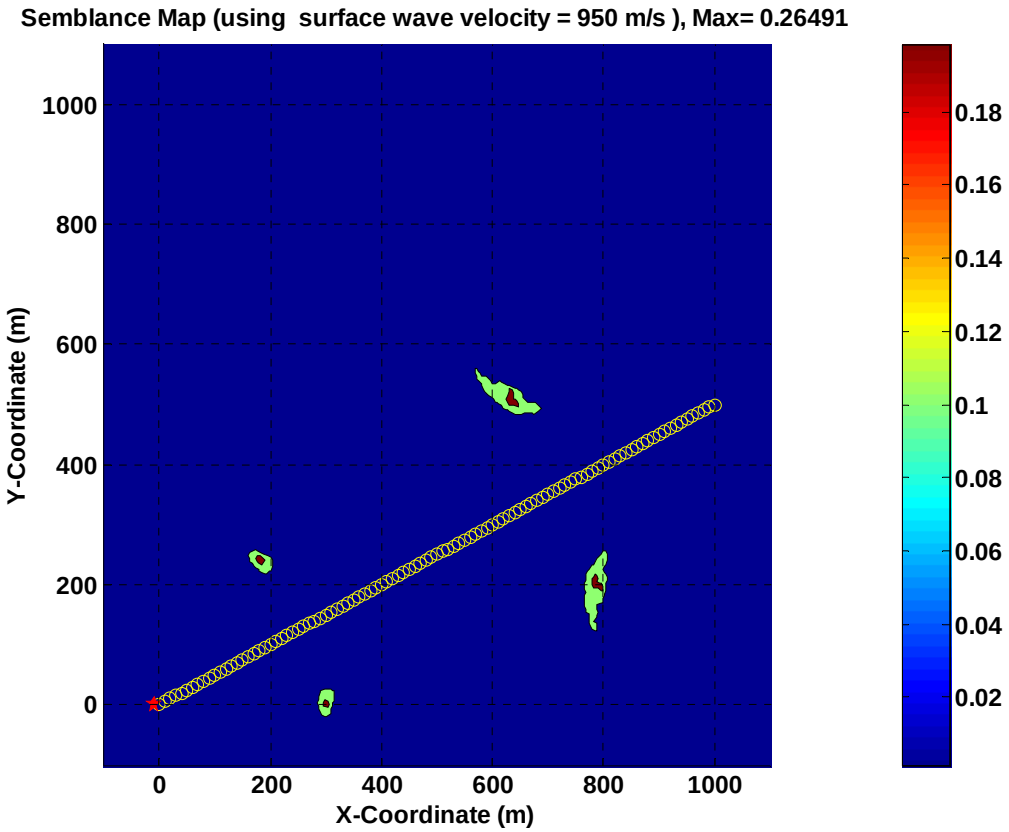

Figure 4- 3: Semblance Map for Line-1 of Model A using surface wave velocity V=950 m/s.

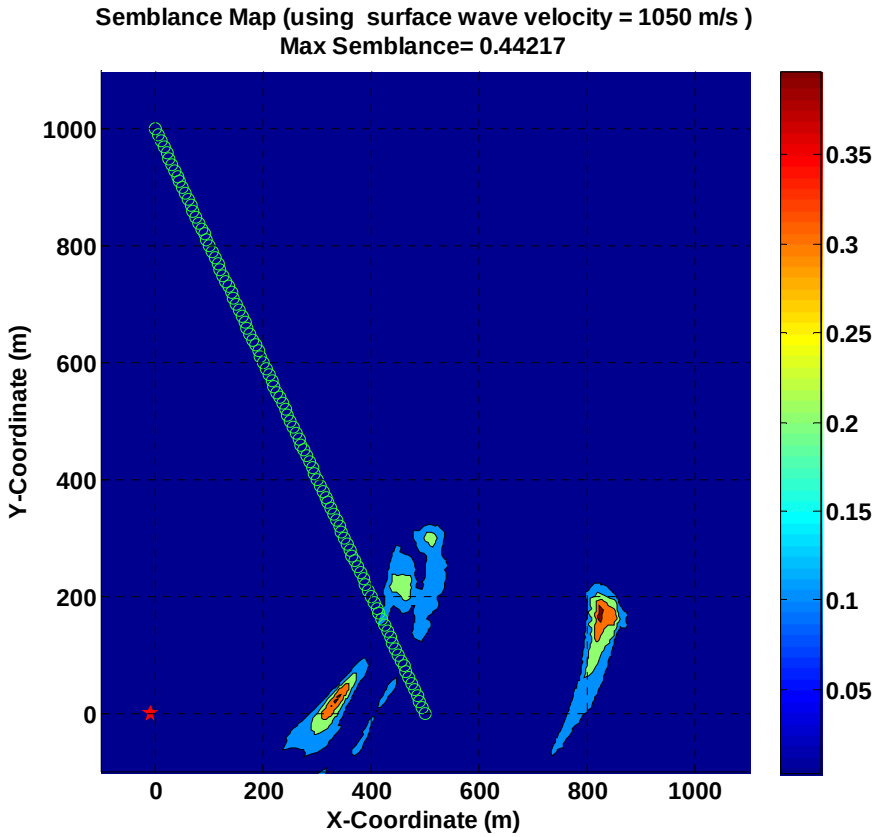

Figure 4- 4: Semblance Map for Line-2 of Model A using surface wave velocity V=1050 m/s.

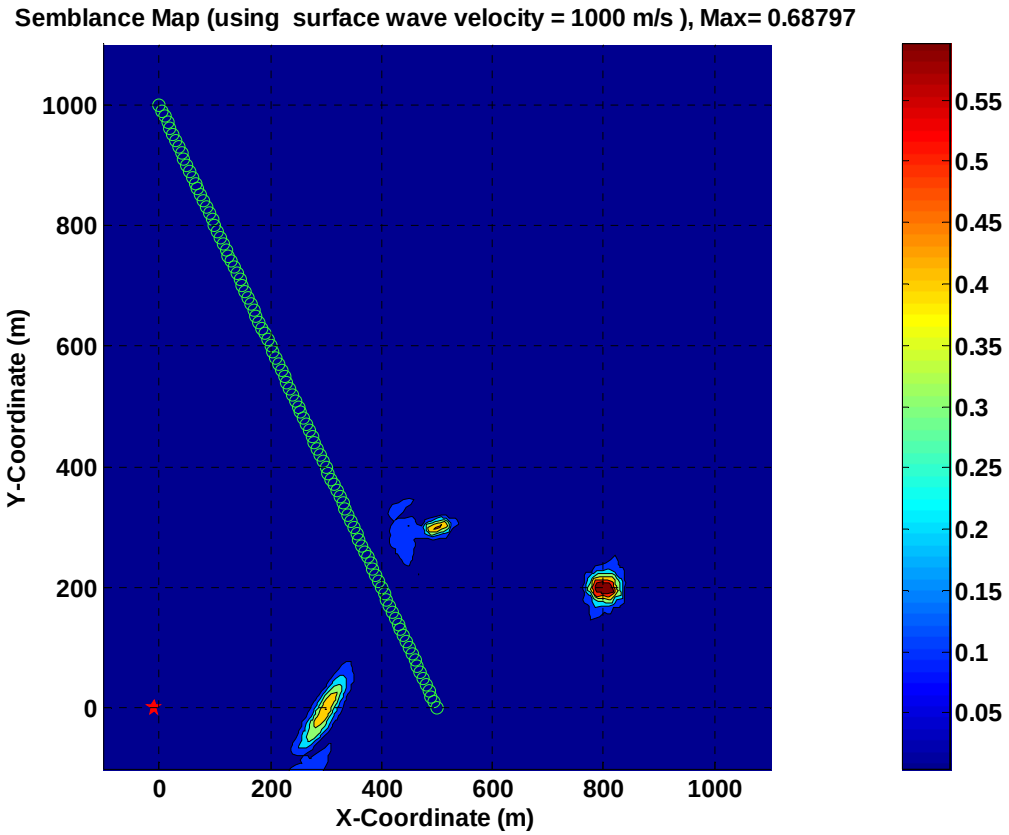

Figure 4- 5: Semblance Map for Line-2 of Model A using surface wave velocity V=1000 m/s.

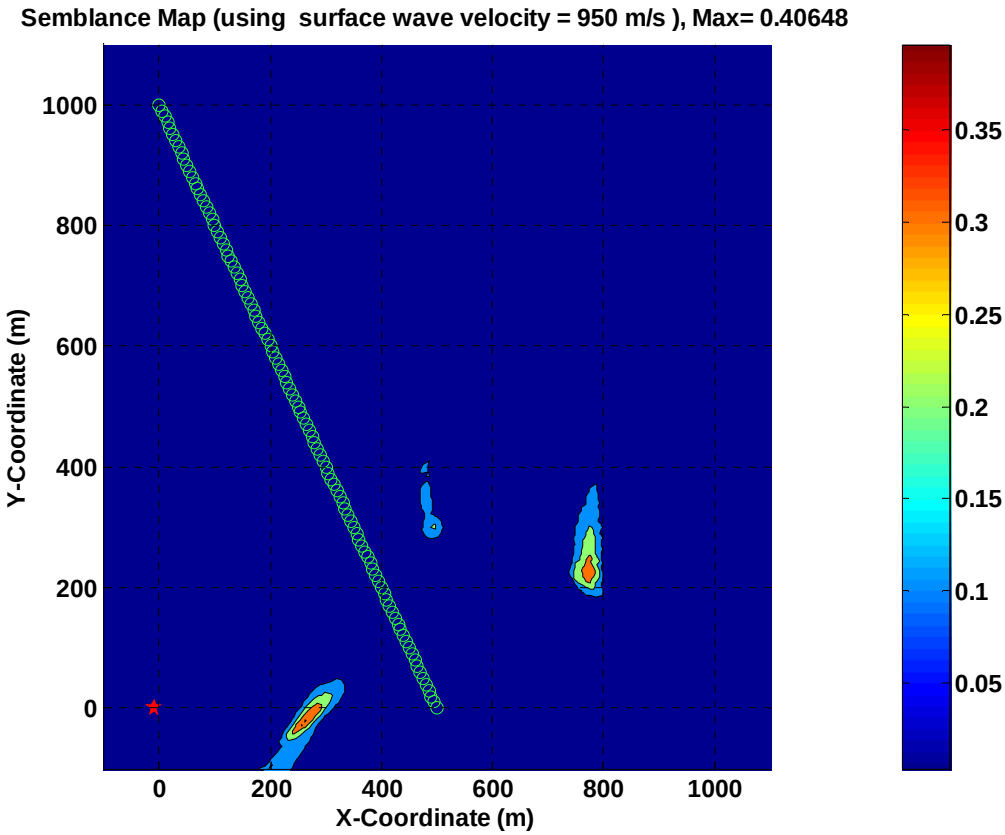

Figure 4- 6: Semblance Map for Line-2 of Model A using surface wave velocity V=950 m/s.

Concentrating on the Semblance Maps with the highest semblance values for Line-1 and Line-2 (Figure 4-2 and Figure 4-5) the diffractors can be picked. But on Line-1 (Figure 4-2) we note that the Code mapped all of the three diffractors in their right locations but also with a mirror image around the axis of the receivers line (see

Table 4- 2) while in Line-2 it didn't mirror image them (see the zoomed Maps in Figure 4-7 & Figure 4-8). This is because the seismic source in Line-1 is in the line of receivers. In this case whether the diffractor is located above or below the receiver line axis, the

total distance from the source to the diffractor and from the diffractor to the receiver will be the same and Equation 2-2 will give the same T(X) curve. This will not happen when the seismic source is offset from the receiver line as in the case of Line-2 where we did not have this ambiguity. So it is better to avoid using shot gathers with the source in the line of receivers or at least to use another line to supplement it. Table 4-2 summarizes the findings of using the Mapping Codes on both shot gathers (Line-1 and Line-2) of Model A. It shows that the estimated diffractor locations from the two shot gathers (in green) are in full agreement with the true diffractor locations from the earth model.

Diffractor Mapping Results of Model A						
Shot Gather	**Figure**	**Velocity (m/s)**	**fsw (Hz)**	**Diffractor**	**Diffractor True Location (x,y)**	**Diffractor Location from Semblance Map (x,y)**
Line-1	**4-2**	**1000**	**15**	**1**	**(300 , 0)**	**(300 , 0) or (180, 240)**
				2	**(500, 300)**	**(500, 300) or (540, 220)**
				3	**(800, 200)**	**(800, 200) or (640, 520)**
Line-2	**4-5**	**1000**	**15**	**1**	**(300 , 0)**	**(300 , 0)**
				2	**(500, 300)**	**(500, 300)**
				3	**(800, 200)**	**(800, 200)**

Table 4- 2: Diffraction Mapping Results for Model A using the two shot gathers in Line-1 and Lin-2.

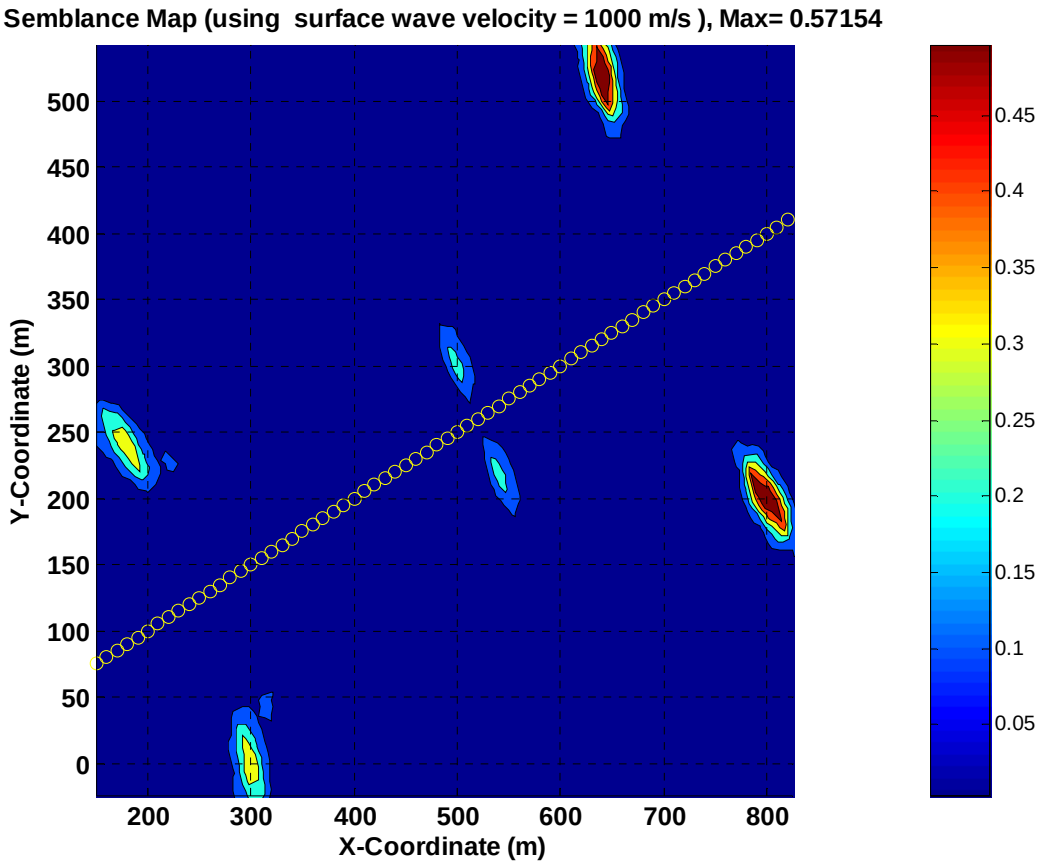

Figure 4- 7: Semblance Map for Line-1 of Model A using surface wave velocity V=1000 m/s (zoomed).

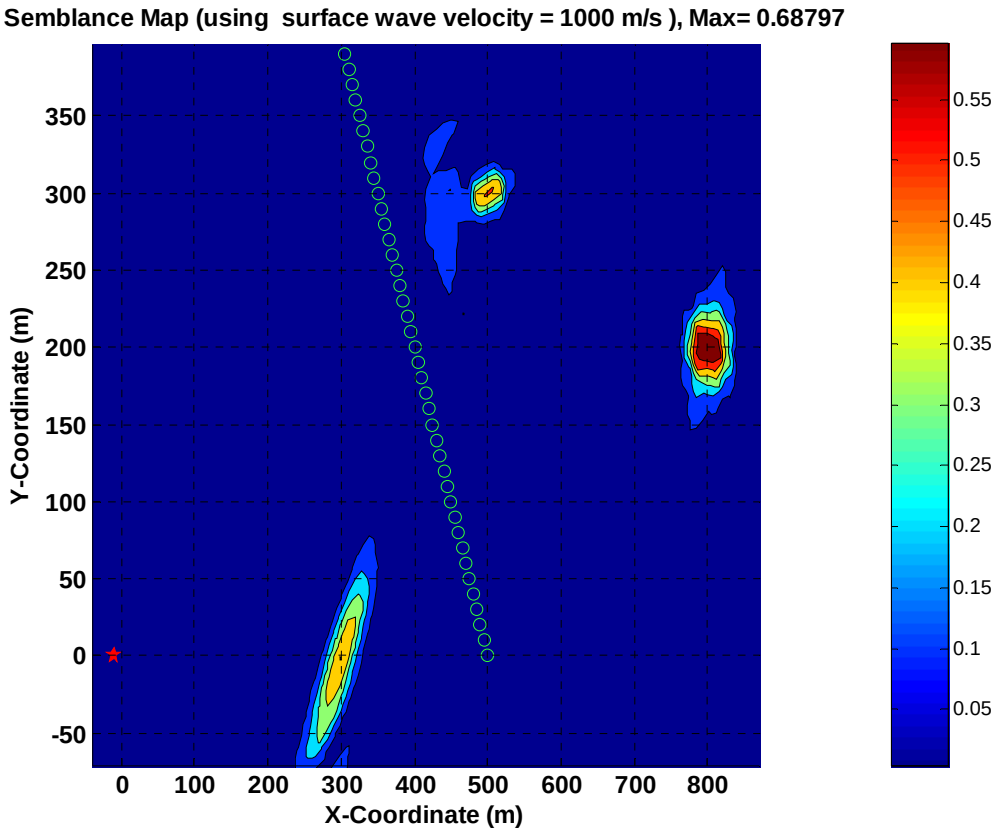

Figure 4- 8: Semblance Map for Line-2 of Model A using surface wave velocity V=1000 m/s (zoomed).

4.2.2 Model B

The two synthetic seismic shot gathers (Line-1 and Line-2) from Earth Model B were used as input to the Mapping Code using three different velocities for surface waves, V=950 m/s, V=900 m/s (the true model velocity), and V=850 m/s with frequency $fsw = 15Hz$. The Code again generated three Semblance Maps for each shot gather, one for each velocity (Figures 4-9 to 4-14). Table 4-3 summarizes the results of the six Semblance Maps. We can see that the best Semblance Maps for both shot gathers are the

ones generated using the true velocity, V=900 m/s (the ones with the highest value, Figure 4-10 and Figure 4-13).

Semblance Maps summary for Model B				
Shot Gather	**Figure**	**Velocity (m/s)**	**fsw (Hz)**	**Maximum Semblance Value**
Line-1	**4-7**	**950**	**15**	**0.40**
	4-8	**900**	**15**	**0.50**
	4-9	**850**	**15**	**0.30**
Line-2	**4-10**	**950**	**15**	**0.32**
	4-11	**900**	**15**	**0.51**
	4-12	**850**	**15**	**0.21**

Table 4-3: Semblance Maps summary for Model B.

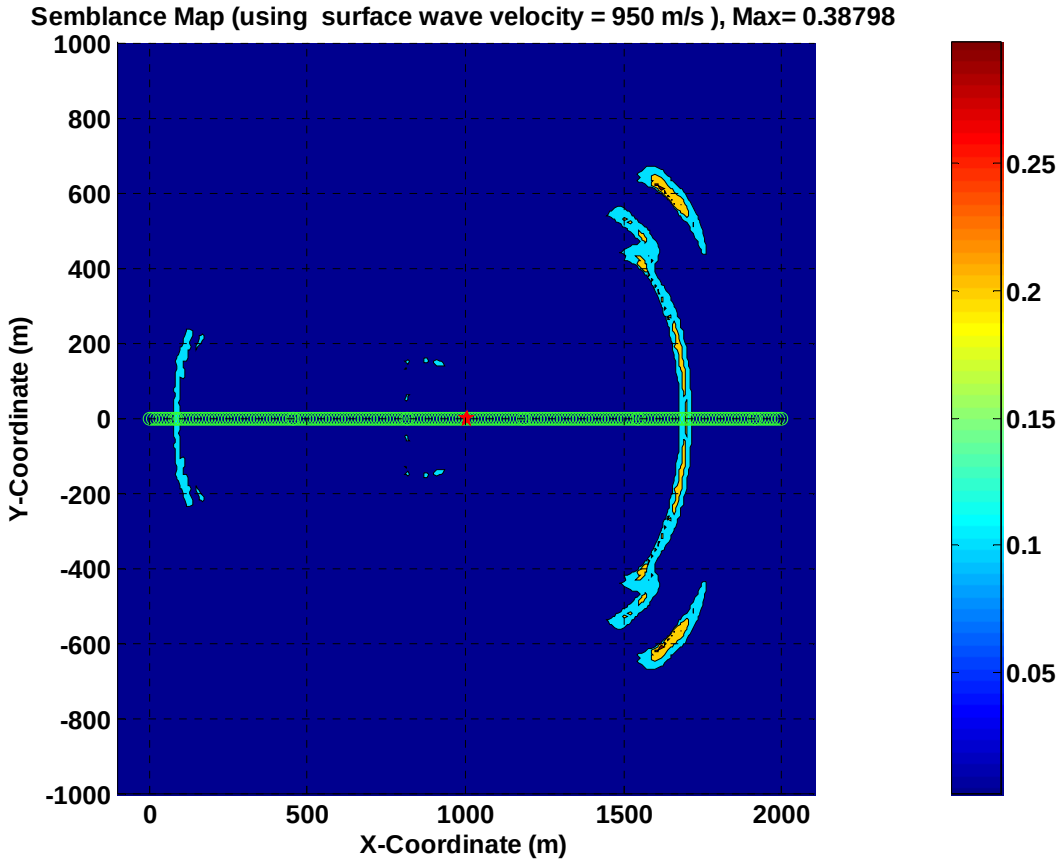

Figure 4- 9: Semblance Map for Line-1 of Model B using surface wave velocity V=950 m/s.

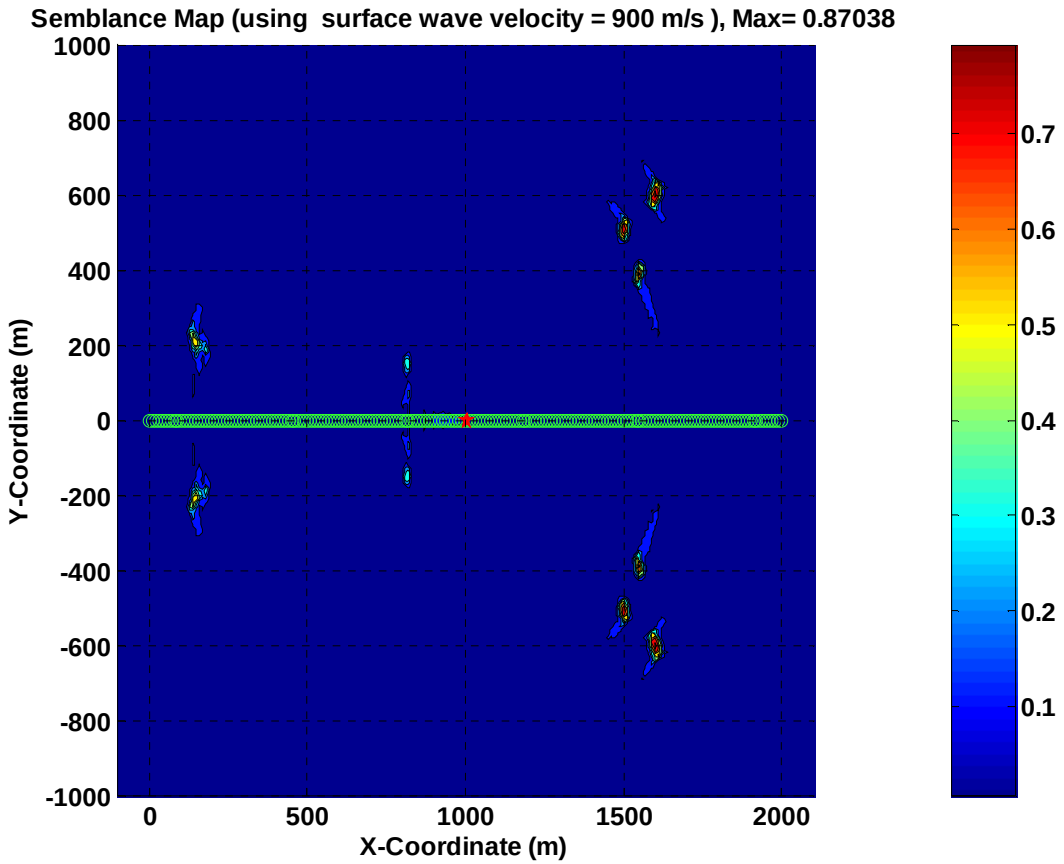

Figure 4- 10: Semblance Map for Line-1 of Model B using surface wave velocity V=900 m/s.

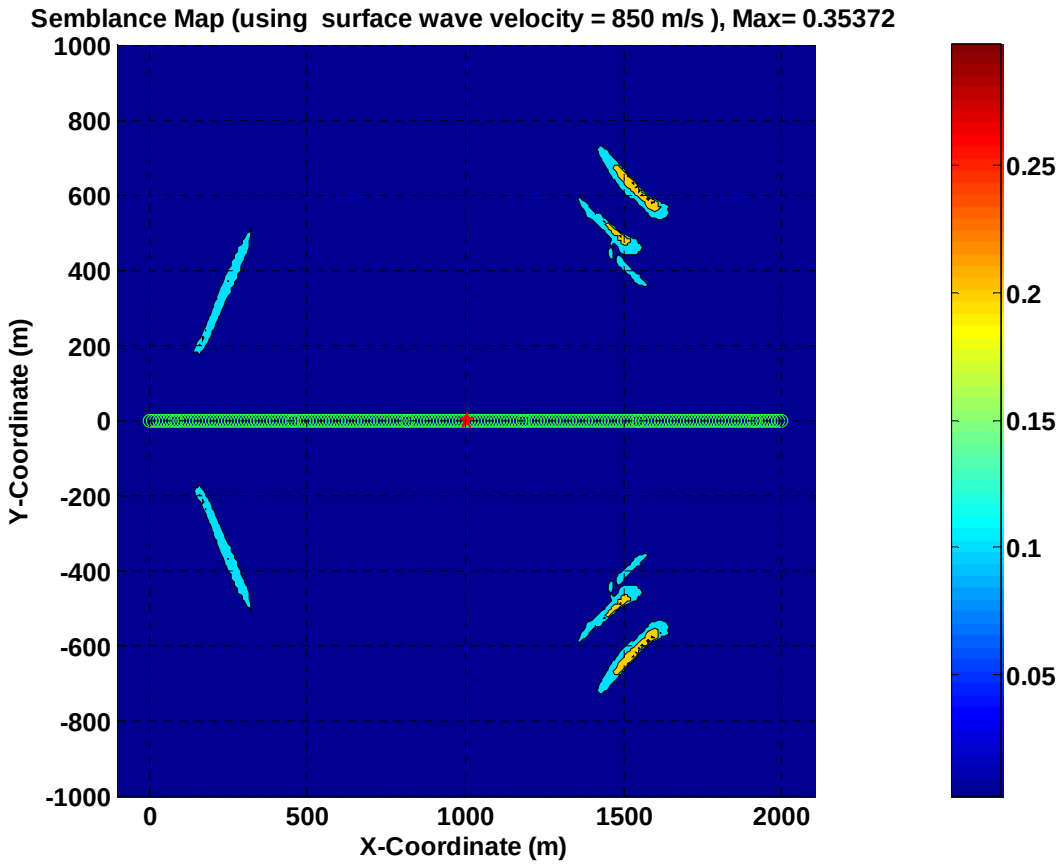

Figure 4- 11: Semblance Map for Line-1 of Model B using surface wave velocity V=850 m/s.

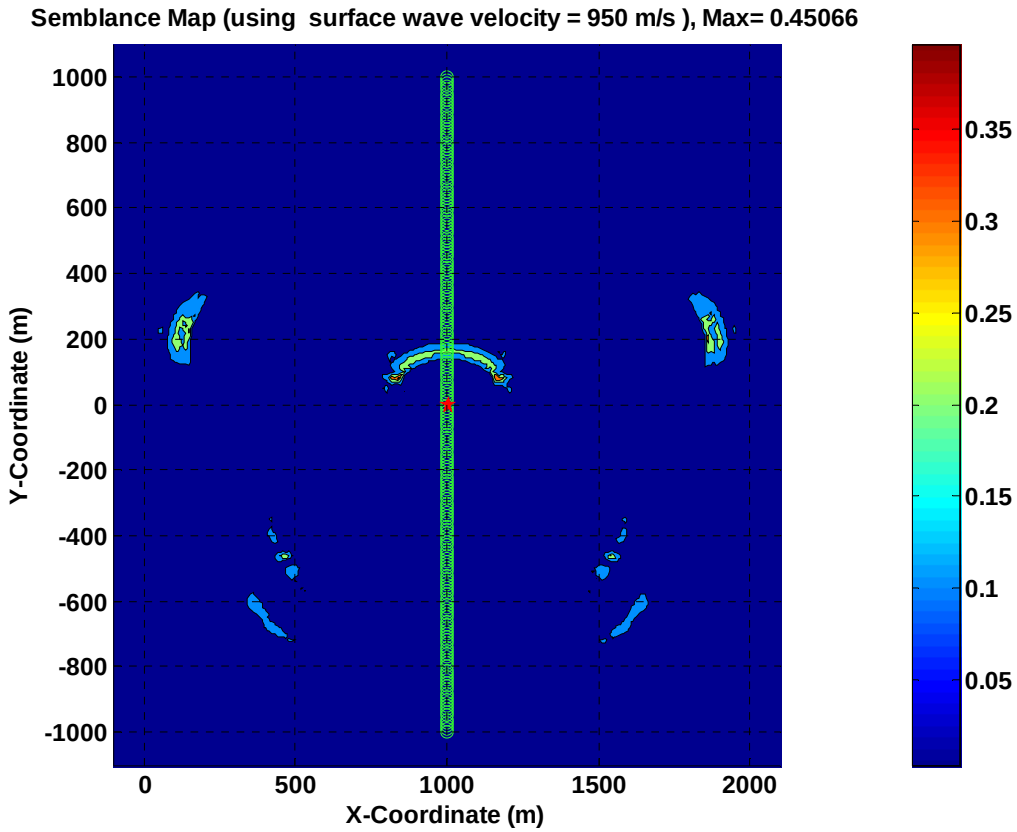

Figure 4- 12: Semblance Map for Line-2 of Model B using surface wave velocity V=950 m/s.

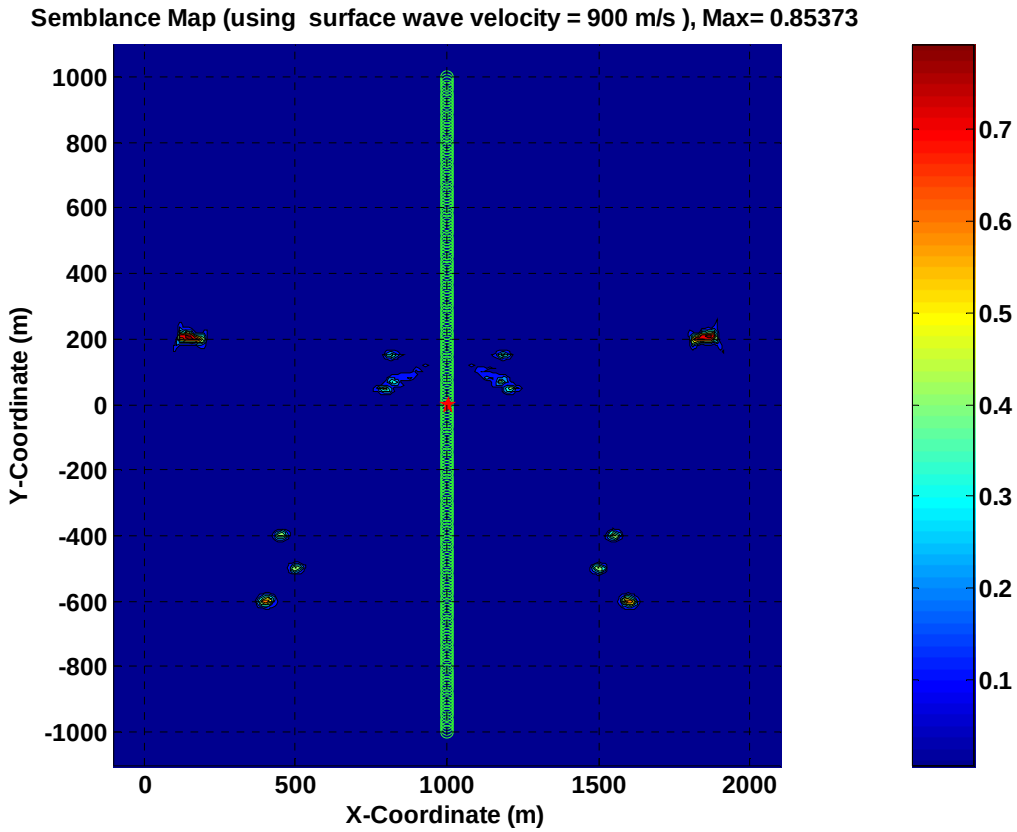

Figure 4- 13: Semblance Map for Line-2 of Model B using surface wave velocity V=900 m/s.

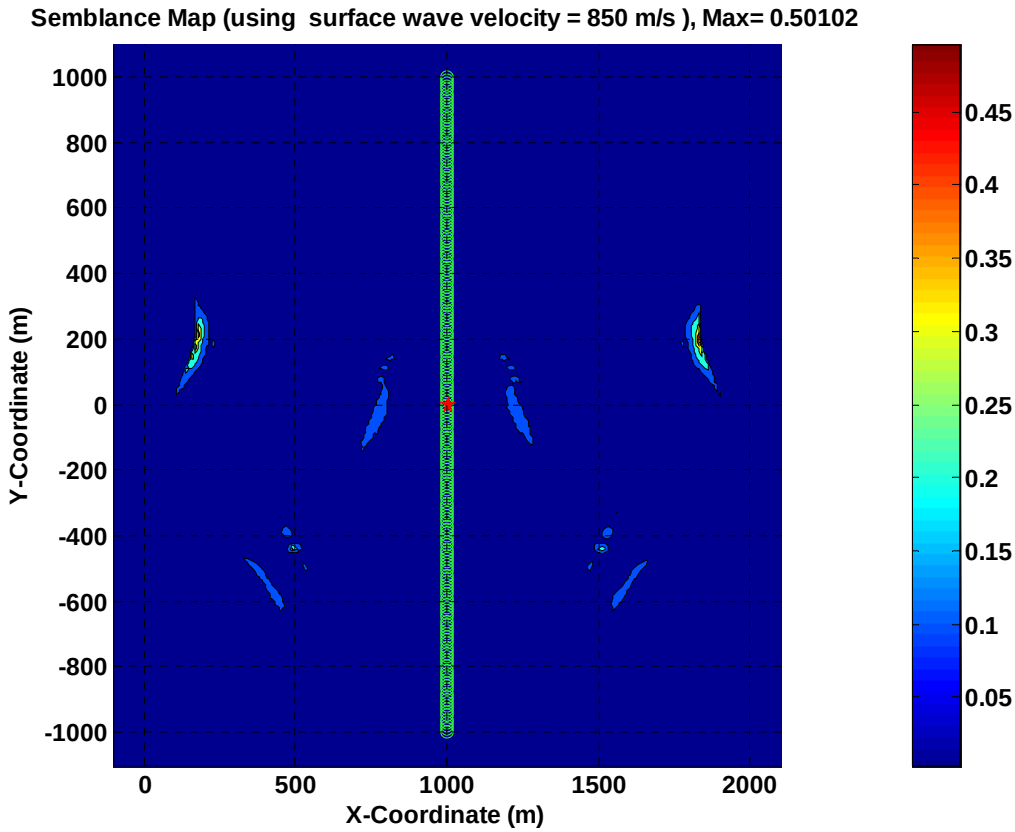

Figure 4- 14: Semblance Map for Line-2 of Model B using surface wave velocity V=850 m/s.

The Semblance Maps with the highest semblance values for Line-1 and Line-2 (Figures 4-10 and 4-13) show that for both lines the Code mapped all of the three clusters of diffractors with a mirror image around the axes of the receivers lines. This ambiguity was expected from previous results as both lines now have their sources within the receiver line. However, because we have two different receiver lines the mirror images of the diffractor clusters will be in different positions while the right positions will be common

in both maps. Utilizing the two Semblance Maps (Figures 4-10 and 4-13) we can pick the right positions of the diffractor clusters.

To evaluate the performance of the Mapping code in term of spatial resolution we need to look at the individual diffractors in each cluster. For cluster (a), the Mapping Code could not resolve individual diffractors (even on the shot gathers, they can be hardly seen as three diffractors, Figure 3- 7 and Figure 3- 8). This is because the separation between individual diffractors in this cluster (10-22 m, see Table 3-1) is below the expected wavelength of the surface wave (900 (m/s) ÷ 15 (Hz) = 60 m). In this case, the user will have difficulties to see three distinct diffractors on the Semblance Maps (Figure 4- 15 and Figure 4- 18).

For cluster (b) where the diffractors are from 25-101 m apart (the average is almost one wavelength of surface wave) the Code could resolve individual diffractors on the Semblance Maps with minor errors (Figure 4-16 and Figure 4- 19). The Code easily resolved the diffractors in cluster (c) where they were 111-206 m apart with no errors (Figure 4- 17 and Figure 4- 20).

The resolving power of the Mapping Code depends on the distance between the diffractors; the larger the distance (compared to the surface wave wavelength) the easier for the code to resolve individual diffractors. Table 4- 4 summarizes the findings of using the Mapping Codes on both shot gathers (Line-1 and Line-2) of Model B.

Model B Diffractor Mapping Results							
Shot Gather	**Figure**	**Velocity (m/s)**	**fsw (Hz)**	**Cluster**	**Diffractor**	**Diffractor True Location (x,y)**	**Diffractor Location from Semblance Map (x,y)**
Line-1	**4-10**	**900**	**15**	**a**	**1**	**(150, 200)**	**(145, 210)**
					2	**(150, 210)**	
					3	**(170, 200)**	
				b	**1**	**(800, 50)**	**(800, 40)**
					2	**(820, 65)**	**(820, 50)**
					3	**(815, 150)**	**(815, 150)**
				c	**1**	**(1500, -500)**	**(1500,-510)**
					2	**(1550, -400)**	**(1550, -390)**
					3	**(1600, -600)**	**(1600, -600)**
Line-2	**4-13**	**900**	**15**	**a**	**1**	**(150, 200)**	**(150, 205)**
					2	**(150, 210)**	
					3	**(170, 200)**	
				b	**1**	**(800, 50)**	**(795, 50)**
					2	**(820, 65)**	**(820, 70)**
					3	**(815, 150)**	**(820, 150)**
				c	**1**	**(1500, -500)**	**(1500, -500)**
					2	**(1550, -400)**	**(1550, -400)**
					3	**(1600, -600)**	**(1600, -600)**

Table 4- 4: Diffraction Mapping results for Model B using the shot gathers in Line-1 and Line-2

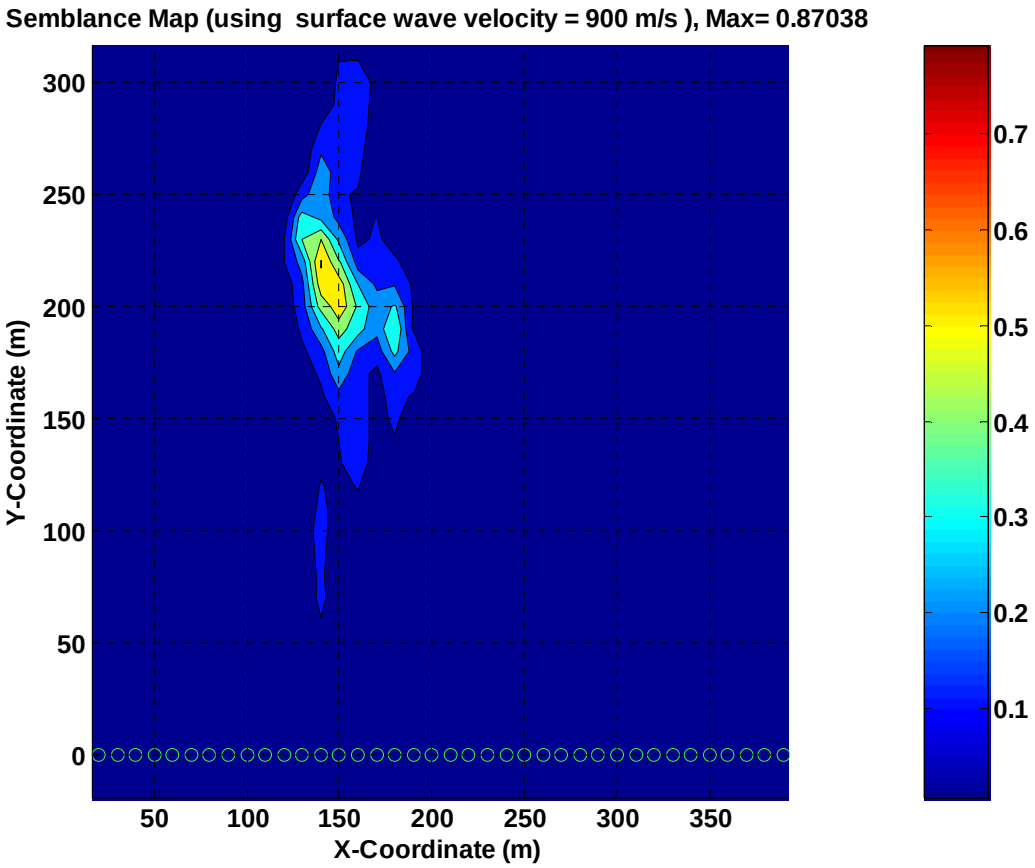

Figure 4- 15: Semblance Map for Line-1 of Model B using surface wave velocity V=900 m/s (zoomed on the common cluster a).

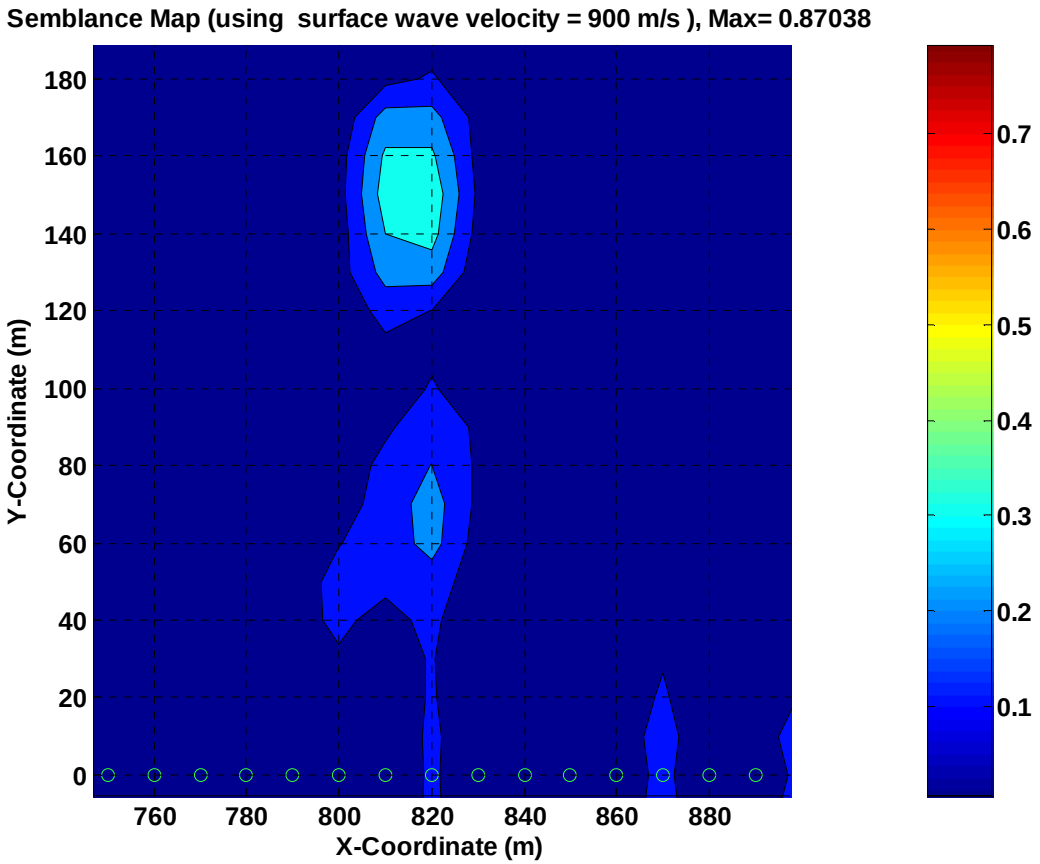

Figure 4- 16: Semblance Map for Line-1 of Model B using surface wave velocity V=900 m/s (zoomed on the common cluster b).

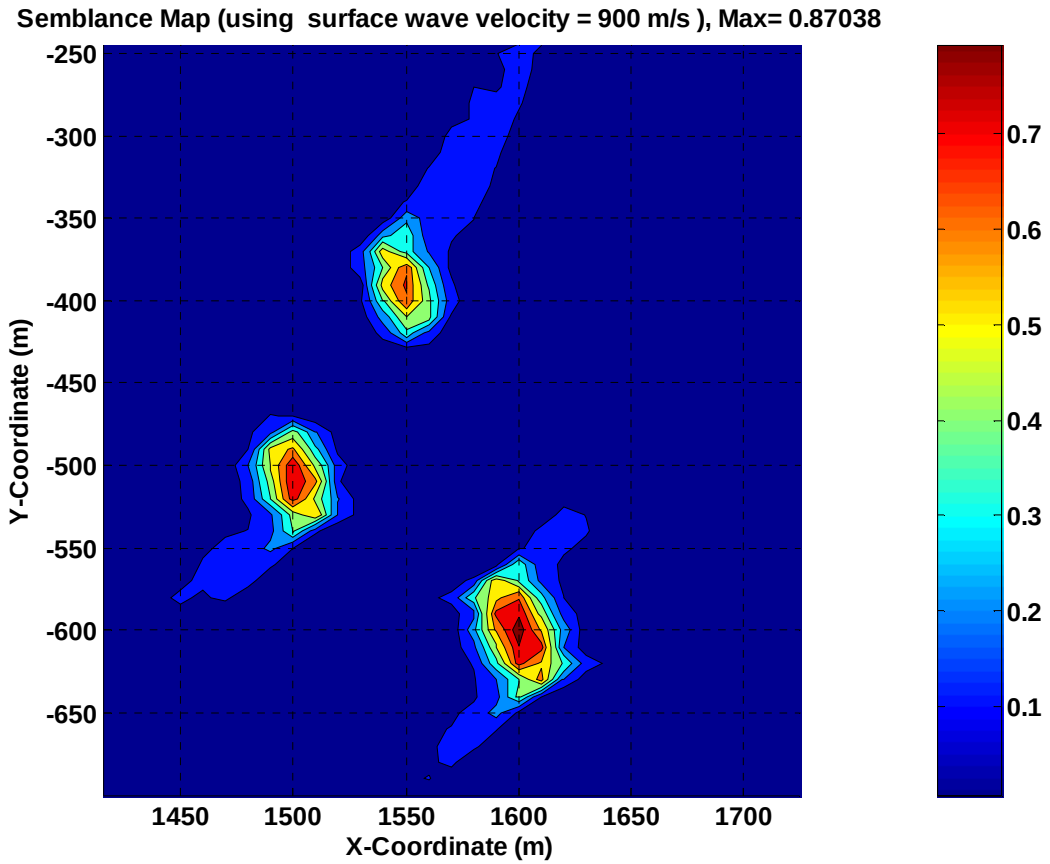

Figure 4- 17: Semblance Map for Line-1 of Model B using surface wave velocity V=900 m/s (zoomed on the common cluster c).

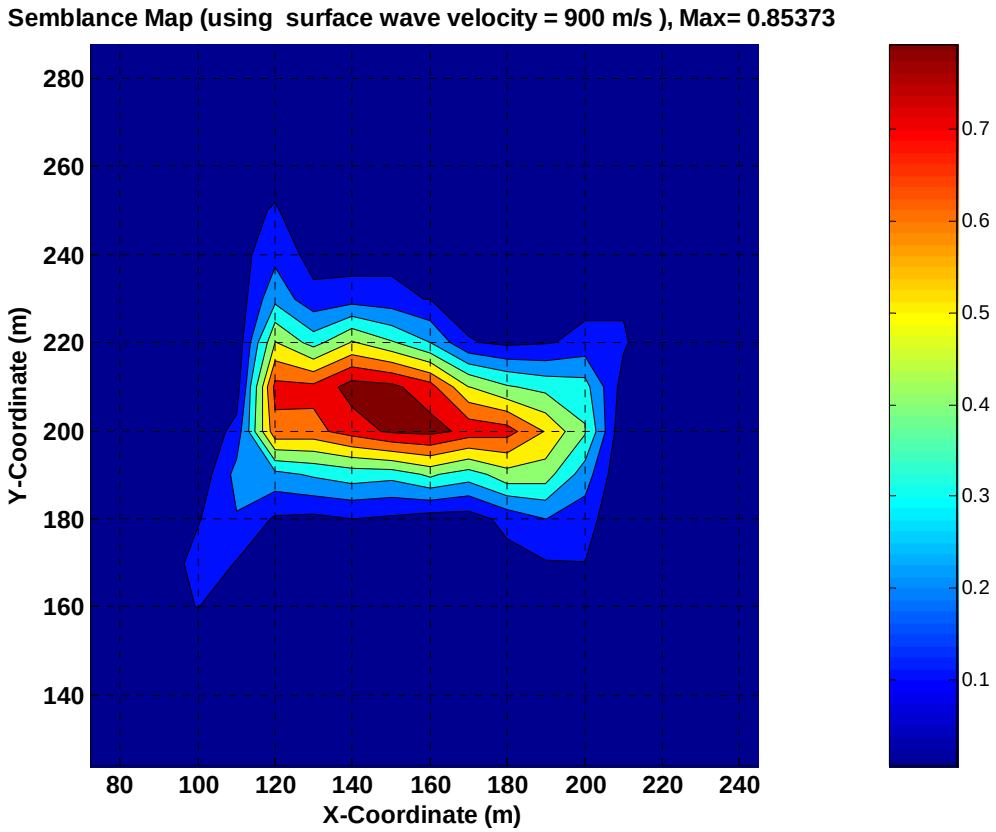

Figure 4- 18: Semblance Map for Line-2 of Model B using surface wave velocity V=900 m/s (zoomed on the common cluster a).

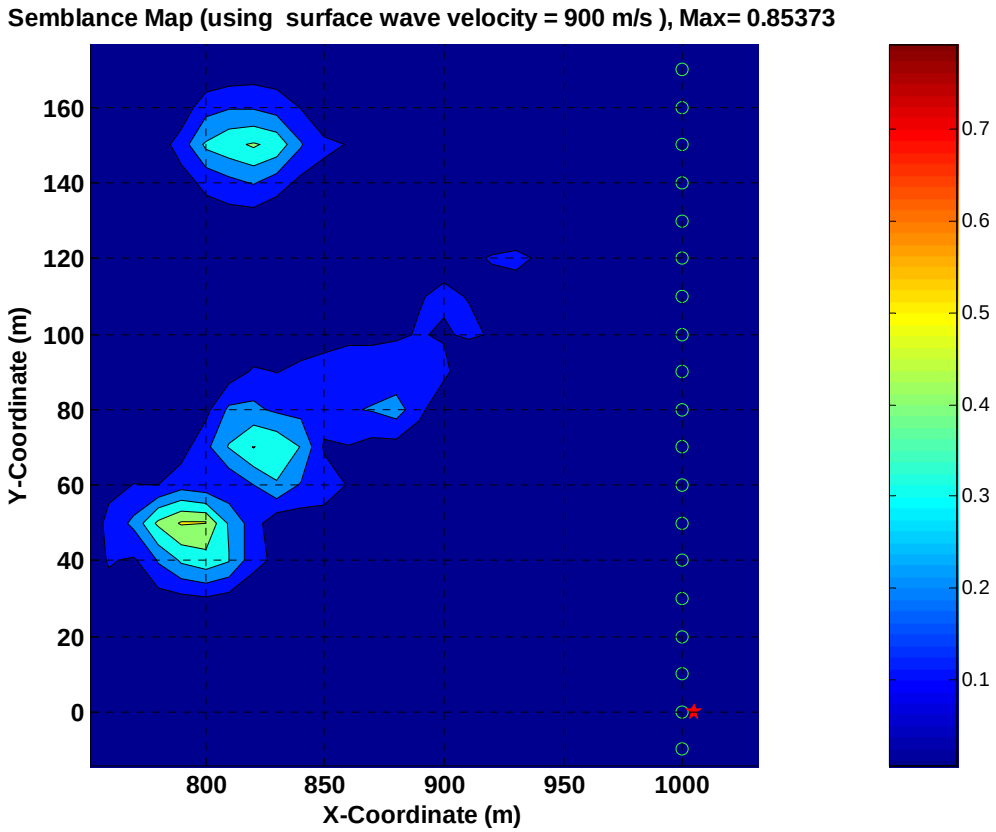

Figure 4- 19: Semblance Map for Line-2 of Model B using surface wave velocity V=900 m/s (zoomed on the common cluster b).

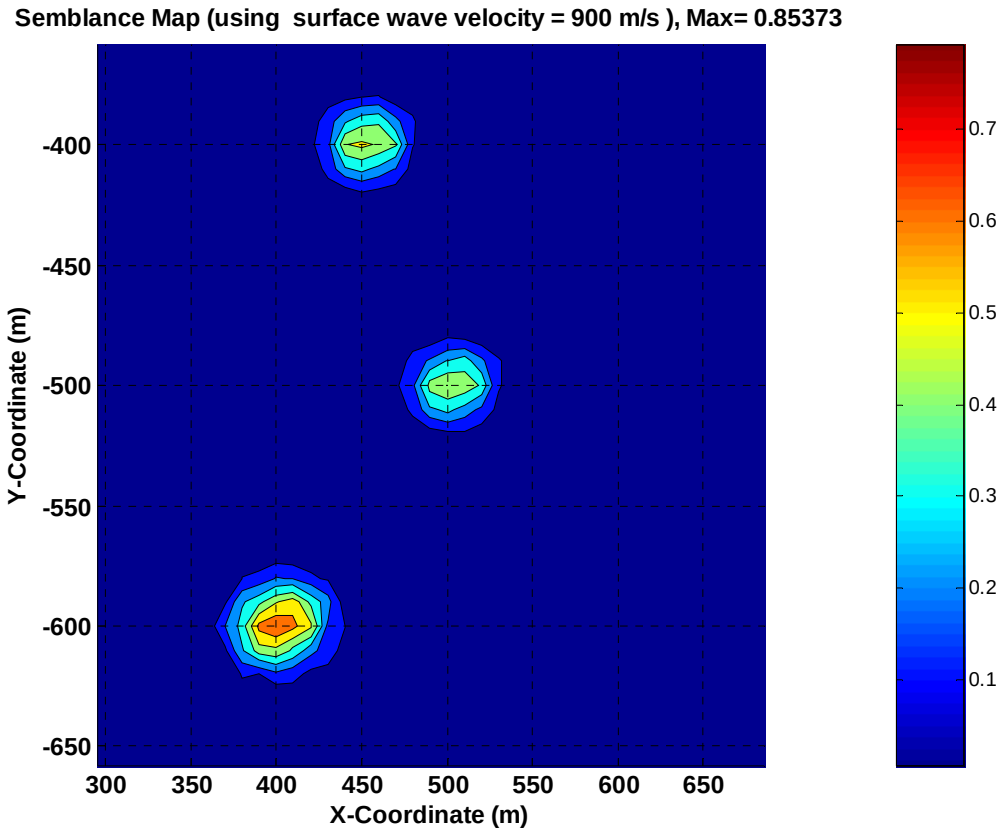

Figure 4- 20: Semblance Map for Line-2 of Model B using surface wave velocity V=900 m/s (zoomed on the common cluster c).

4.3 Attenuation Results

4.3.1 Model A

After the successful mapping of the three diffractors on Model A from the two shot gathers (Line-1 and Line-2), I used the Attenuation Code to attenuate the diffraction events from the three diffractors on both shot gathers. The Code succeeded in estimating

and attenuating the diffractions on both shots, even when the diffractions have minor overlap between them. Results are shown on Figure 4- 21 to Figure 4- 26.

The estimation results of single traces inside the diffractor windows are displayed for two traces of diffractor no.3 of the shot gather Line-1 for Model A (trace no. 75 at the peak of the diffraction hyperbola on Figure 4- 27 and trace no. 20 towards one of the flanks of the hyperbola on Figure 4- 28).

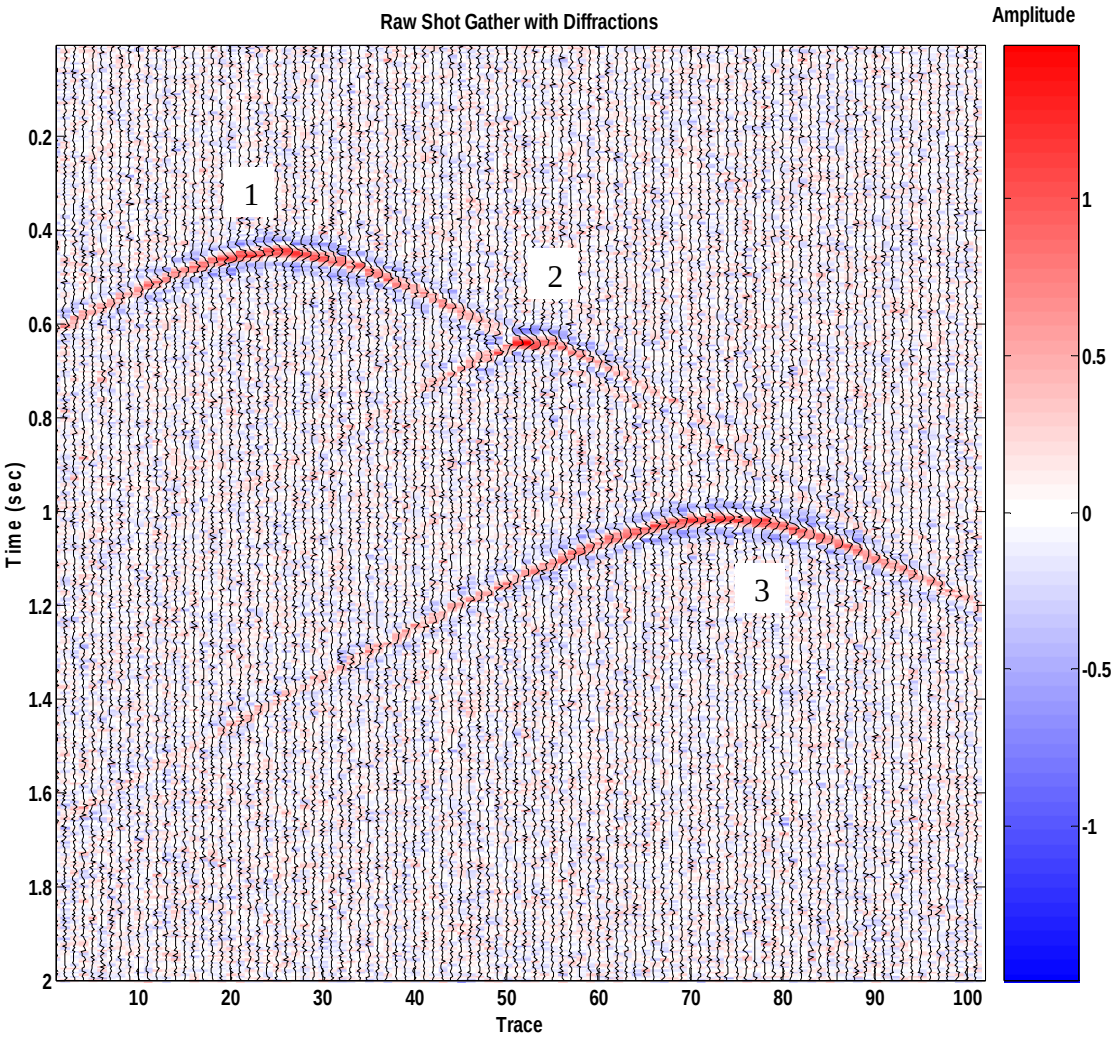

Figure 4- 21: Synthetic shot gather from Line-1 of Model A.

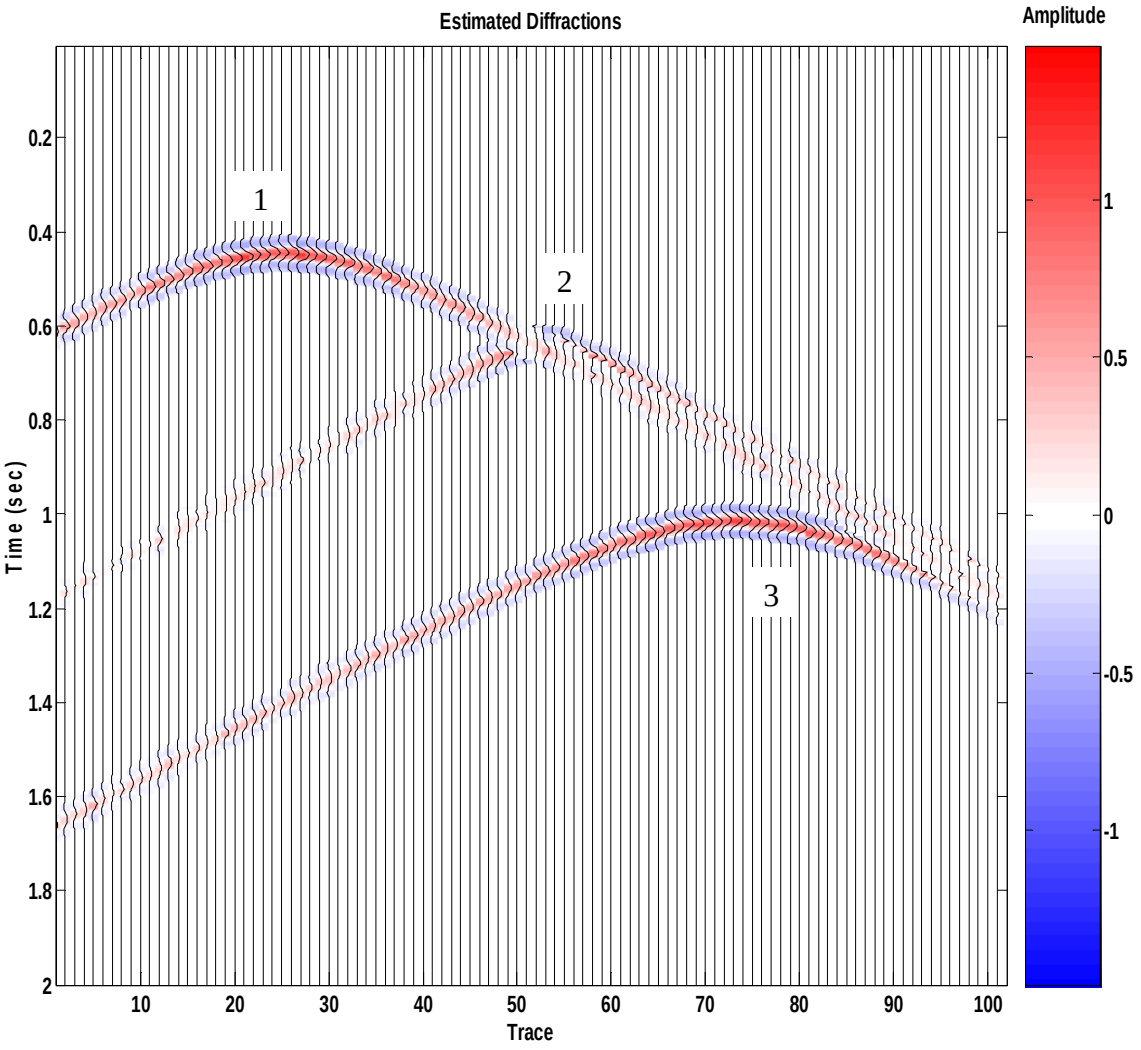

Figure 4- 22: Estimation of the three diffractions from Line-1 of Model A.

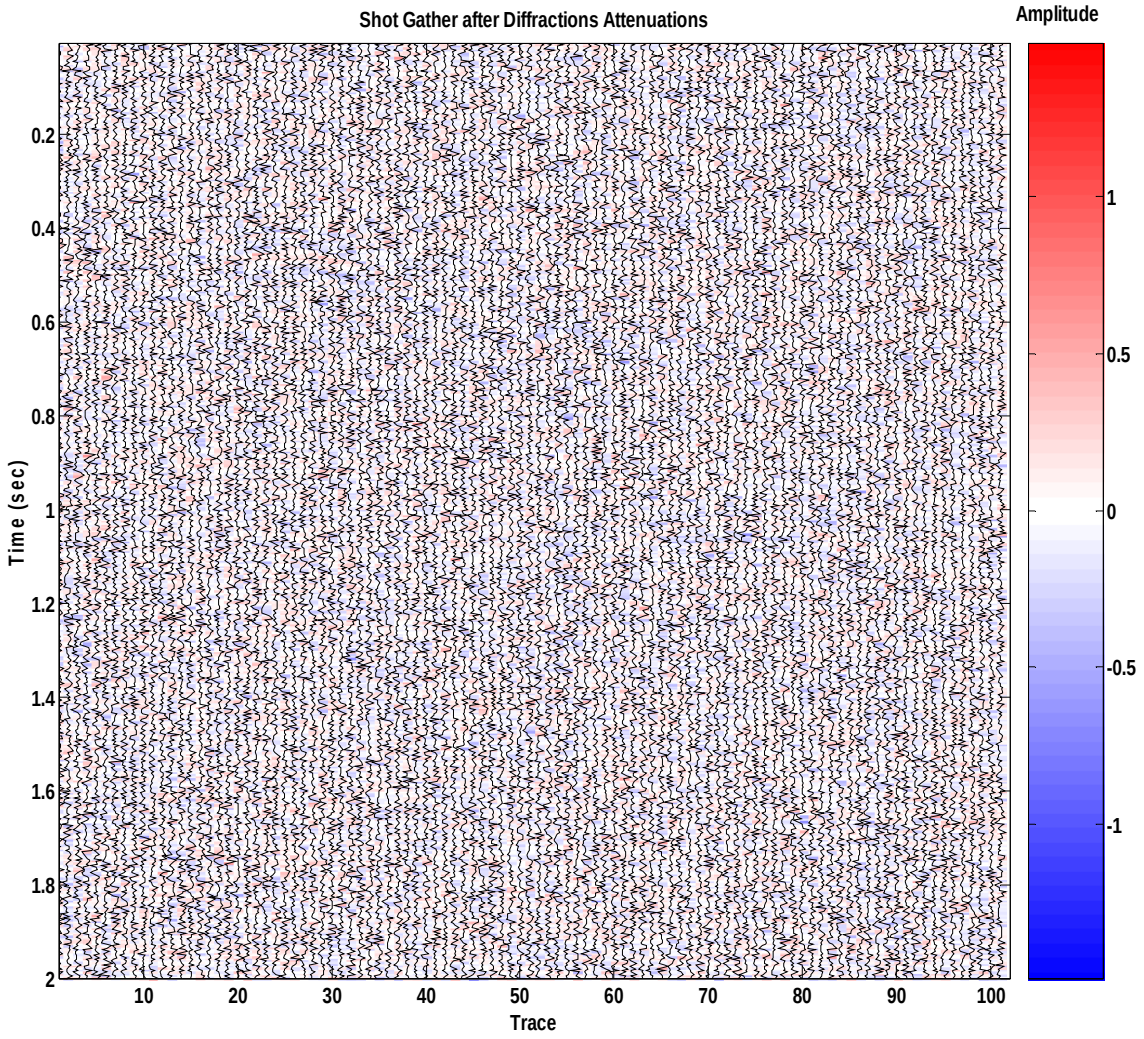

Figure 4- 23: Shot gather Line-1 of Model A after subtracting the estimated diffraction events.

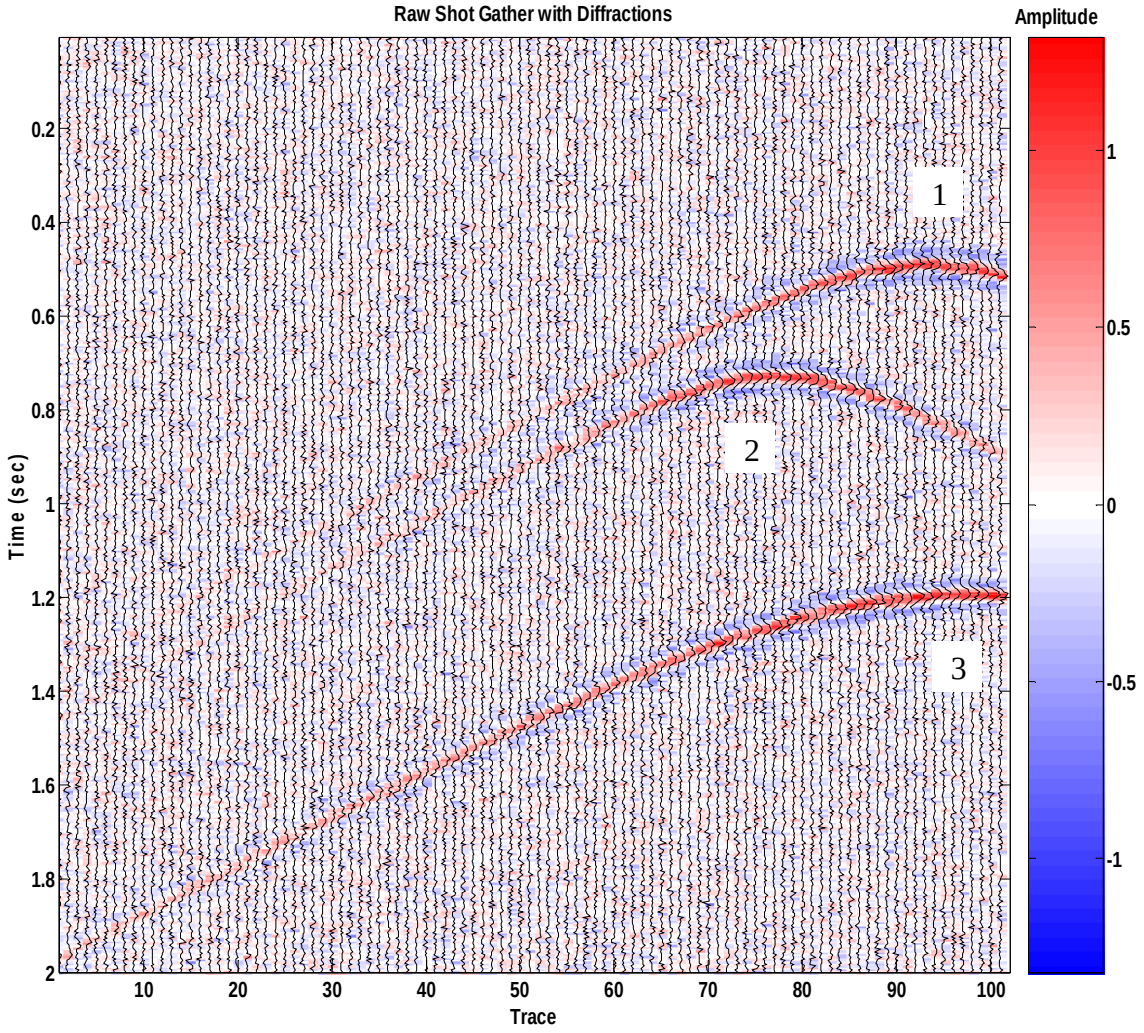

Figure 4- 24: Synthetic shot gather from Line-2 of Model A.

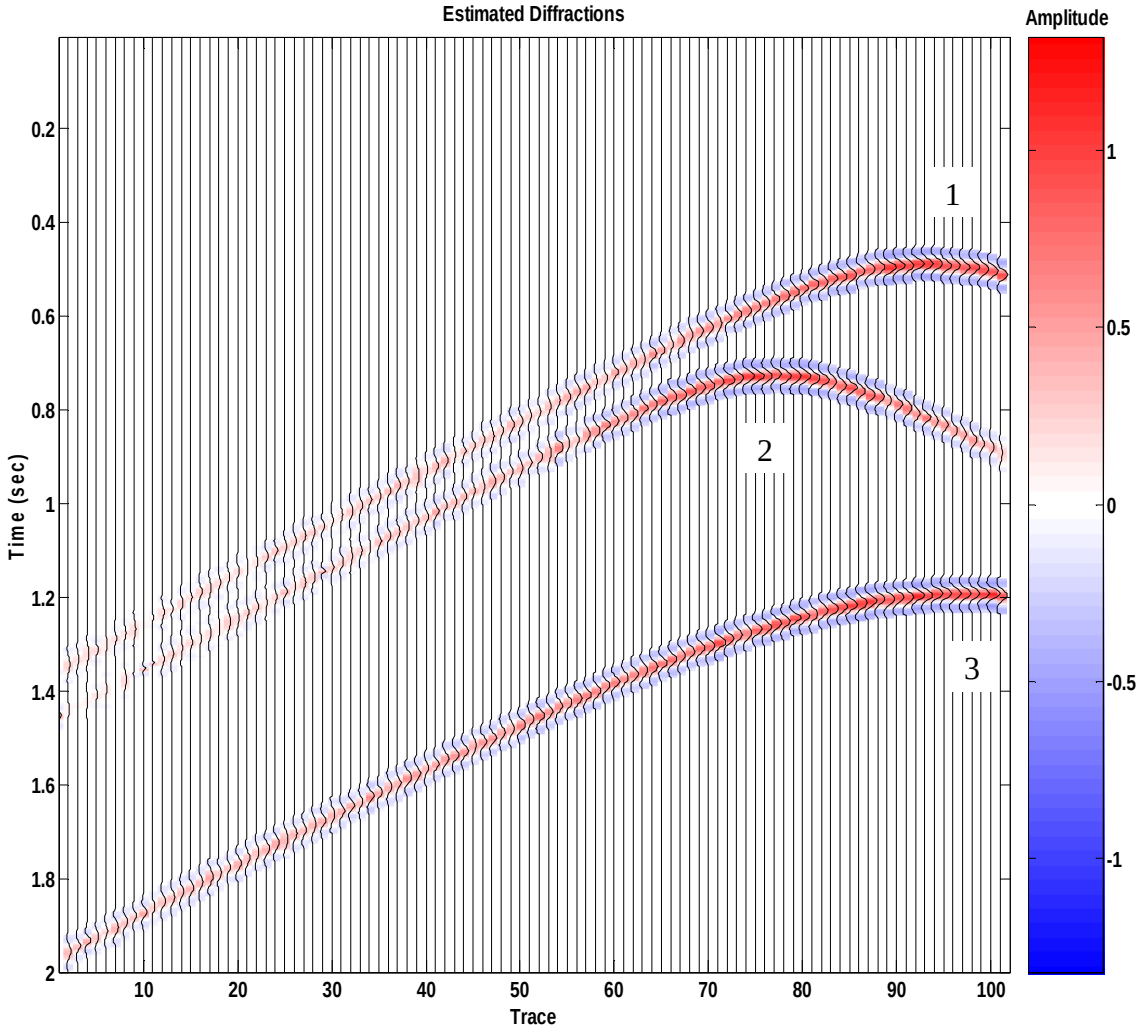

Figure 4- 25: Estimation of the three diffractions from Line-2 of Model A.

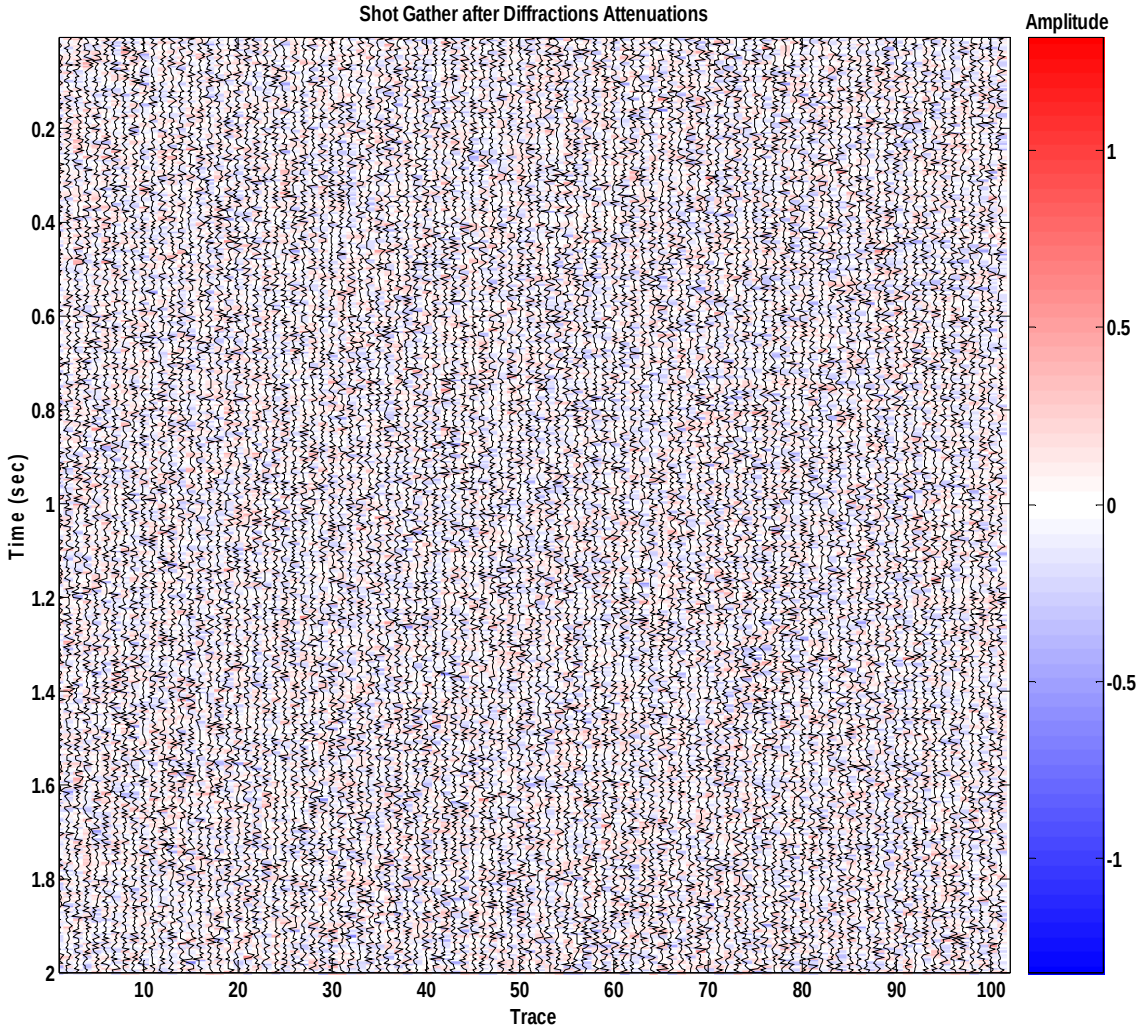

Figure 4- 26: Shot gather Line-2 of Model A after subtracting the estimated diffraction events.

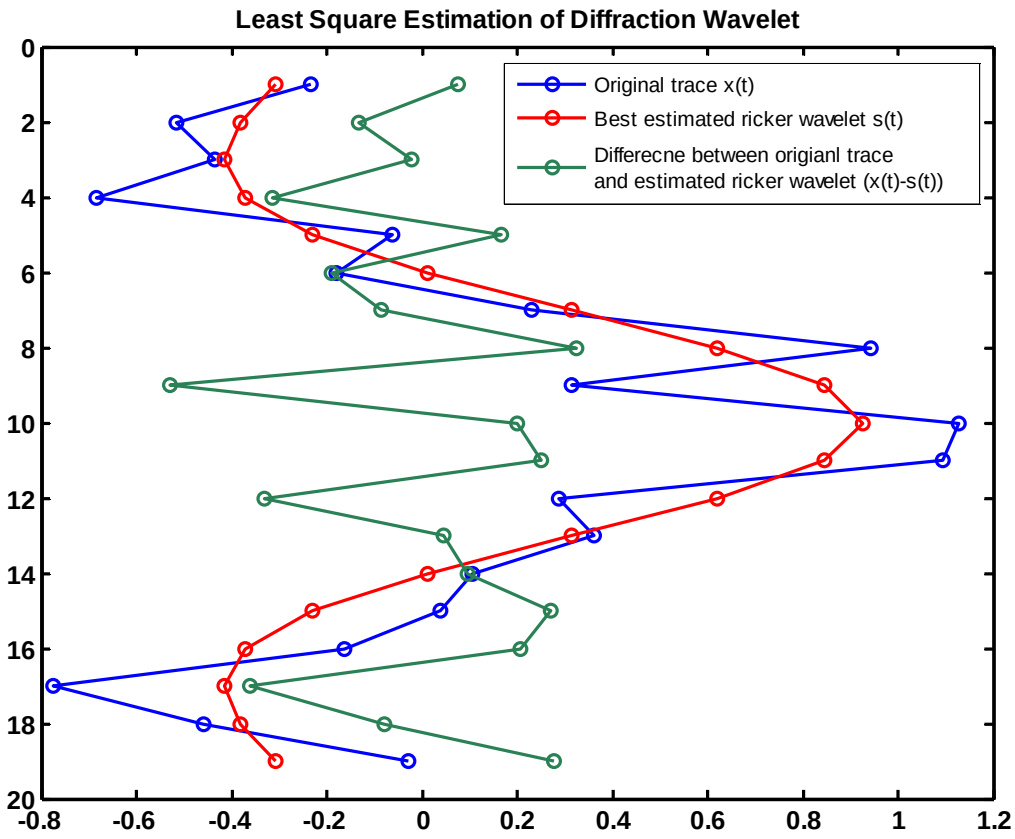

Figure 4- 27: Estimation of Ricker wavelet for trace no. 75 in the window of diffractor no. 3 in Line-1 Model A.

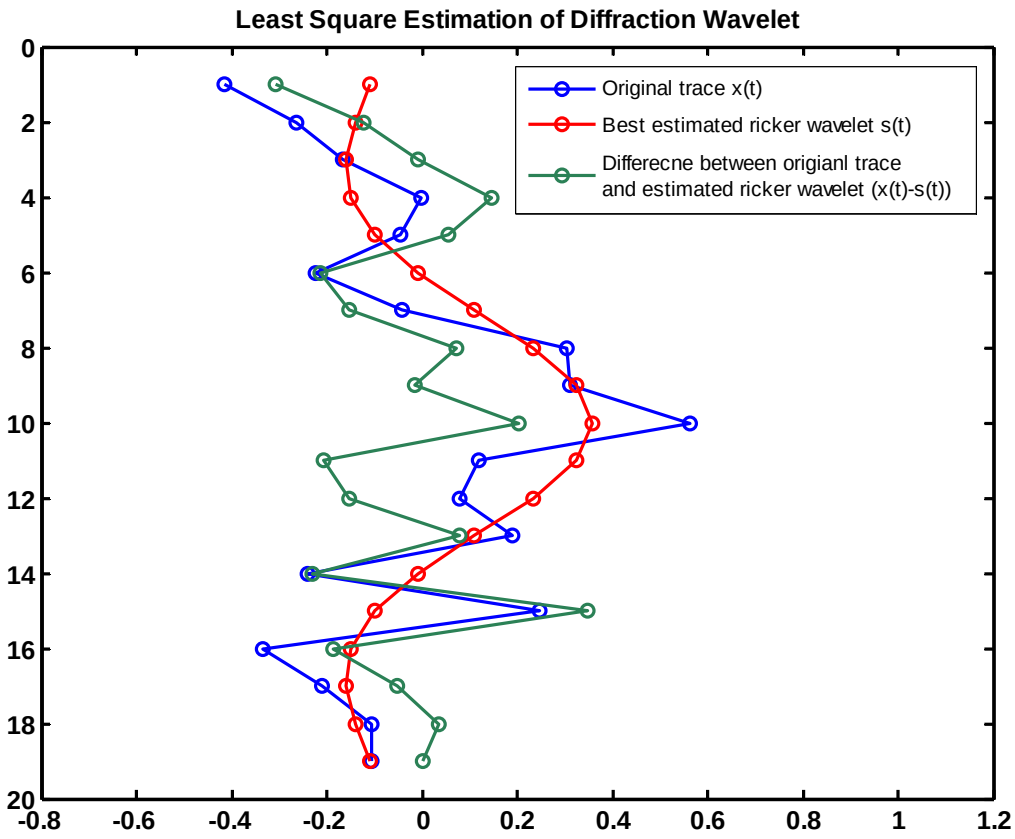

Figure 4- 28: Estimation of Ricker wavelet for trace no. 20 in the window of diffractor no. 3 in Line-1 Model A.

4.3.2 Model B

The Mapping Code results from both shot gathers (Line-1 and Line-2) of Model B were used as input to the Attenuation Code to estimate and attenuate the diffraction events from the three clusters of diffractors. The Code in general did a good job in estimating and attenuating the diffractions especially for clusters (b & c) where the separations between the diffractors are reasonably good on both shots (Figure 4-31 and Figure 4- 34).

Cluster (a) diffractions were the least attenuated because we picked them as one diffractor on the semblance maps (due to the small spatial separation between them).

Re-running the Attenuation Code again on both shots with the true locations of the diffractors in each cluster (the modeled locations), improved the attenuation of cluster (a) diffractors -and the diffractors of the other two clusters. This shows the importance of the careful picking of diffraction locations from the semblance maps.

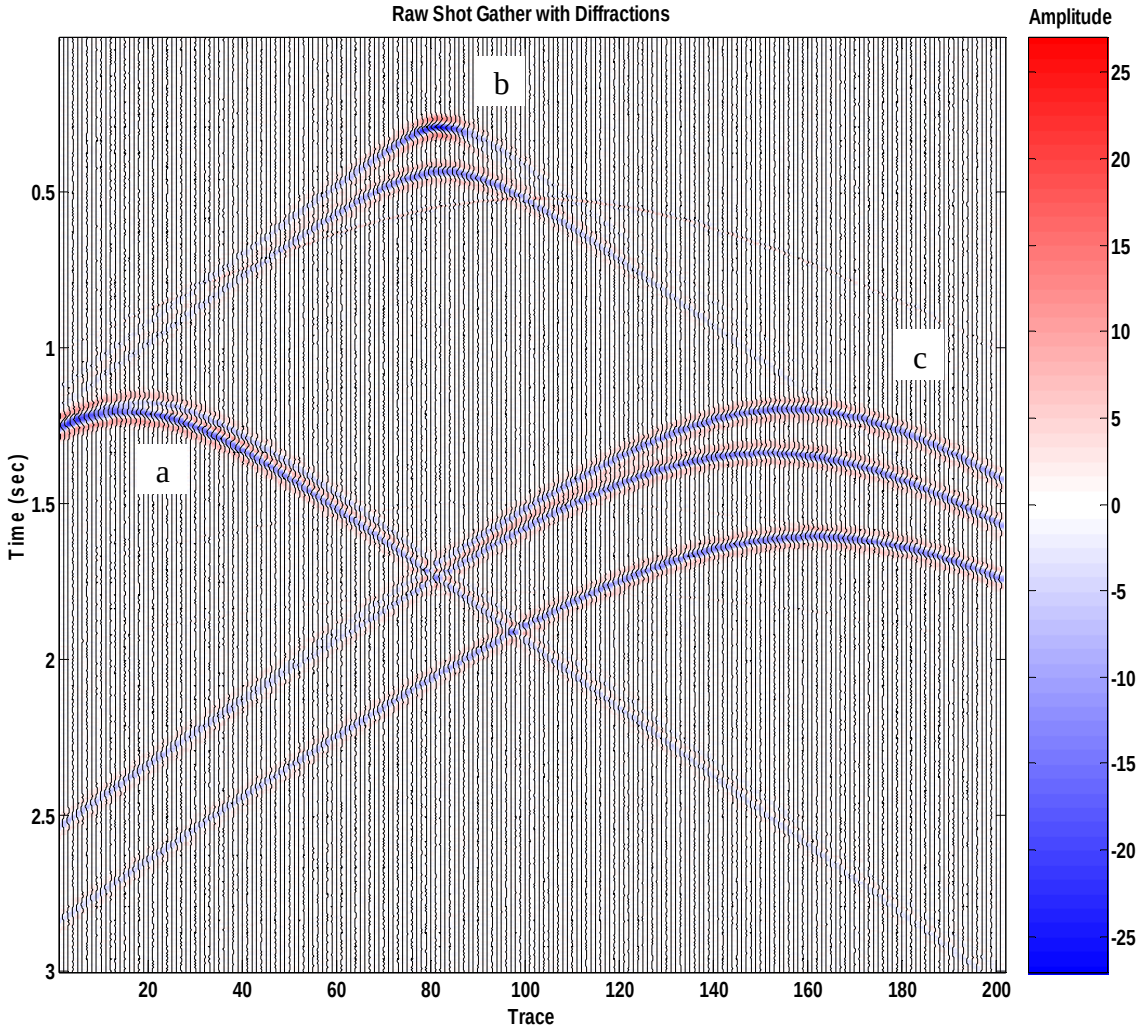

Figure 4- 29: Synthetic shot gather from Line-1 of Model B.

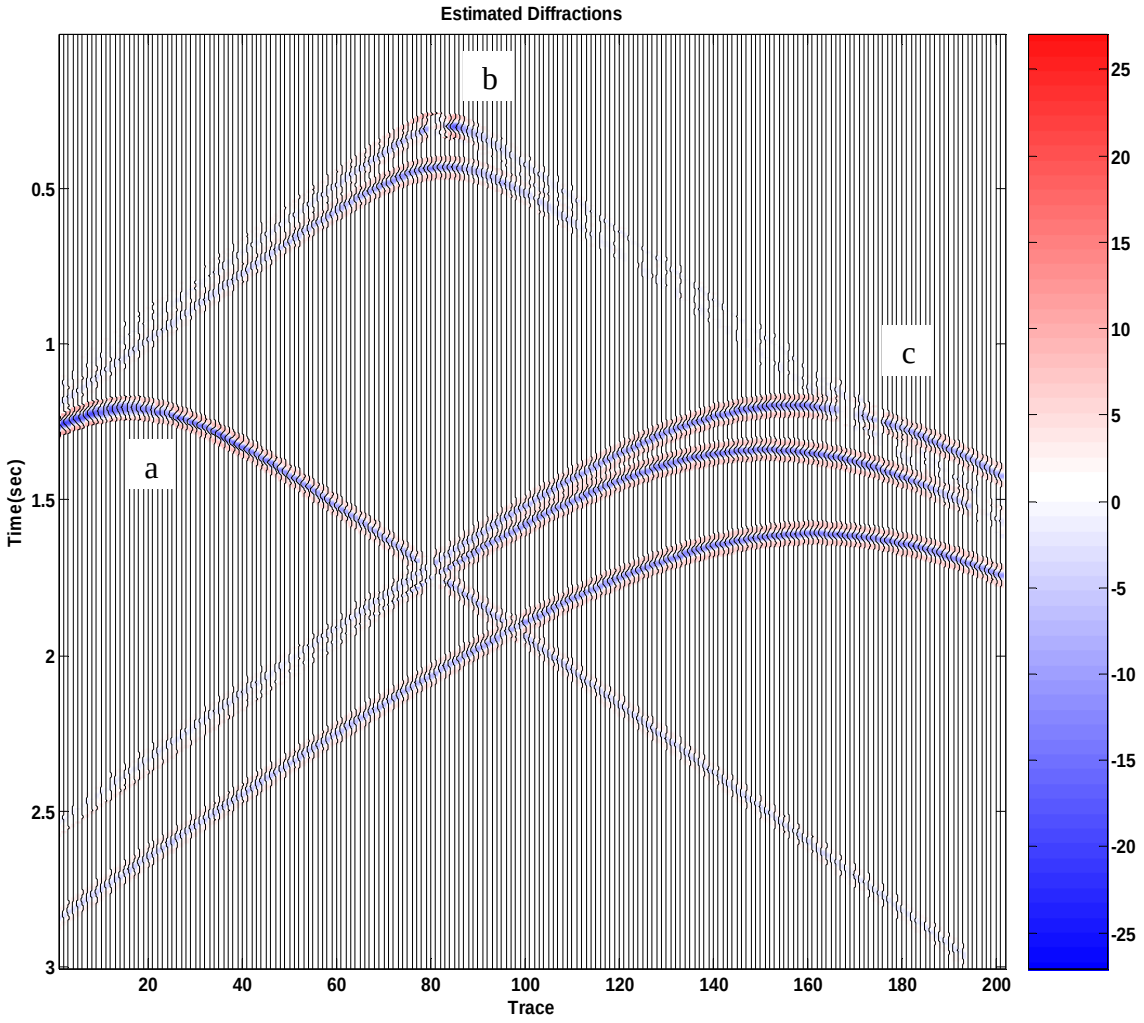

Figure 4- 30: Estimation of the three diffractions clusters from Line-1 of Model B. Note that cluster (a) is picked as one diffractor (see Table 4- 4).

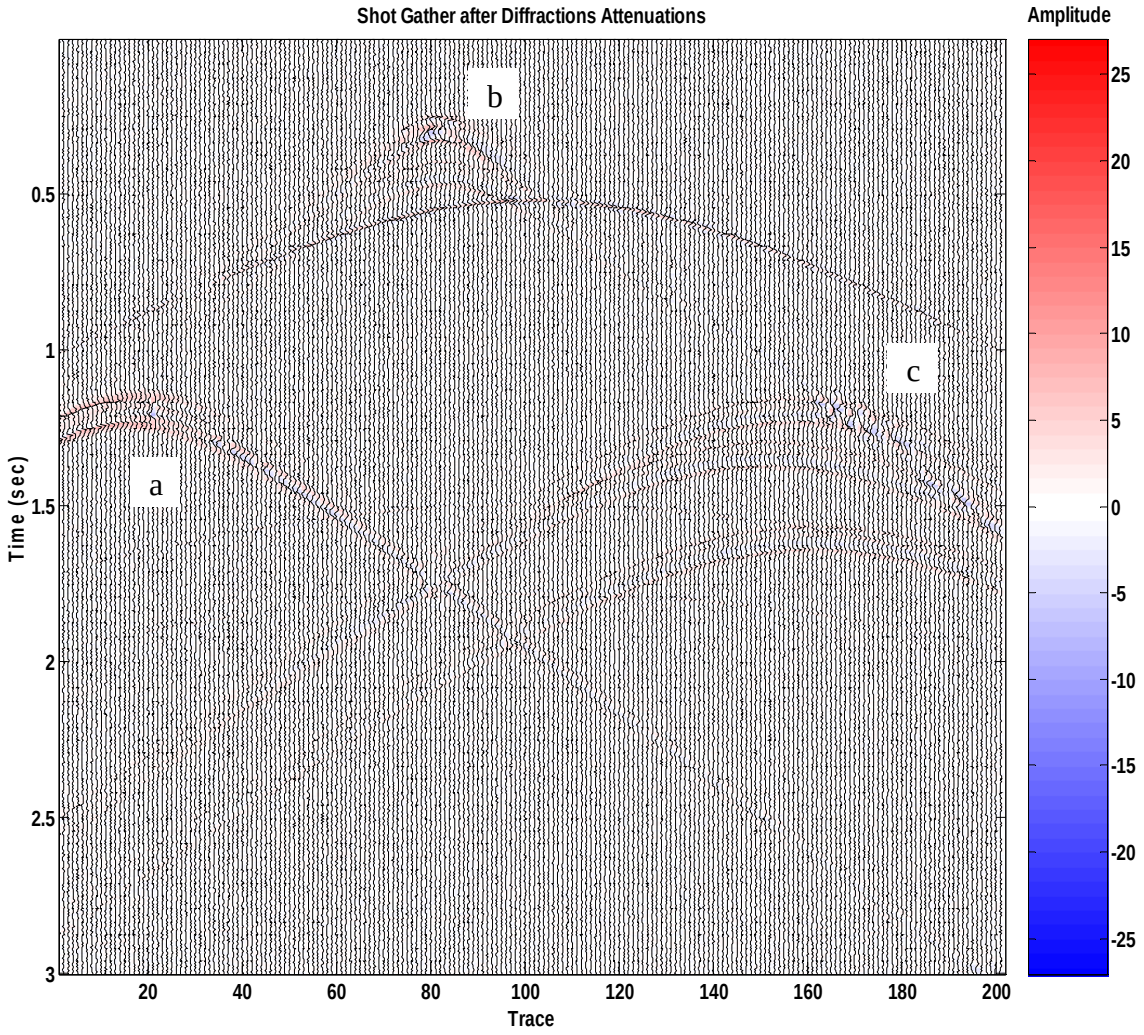

Figure 4-31: Shot gather (Line-1 of Model B) after subtracting the estimated diffraction events.

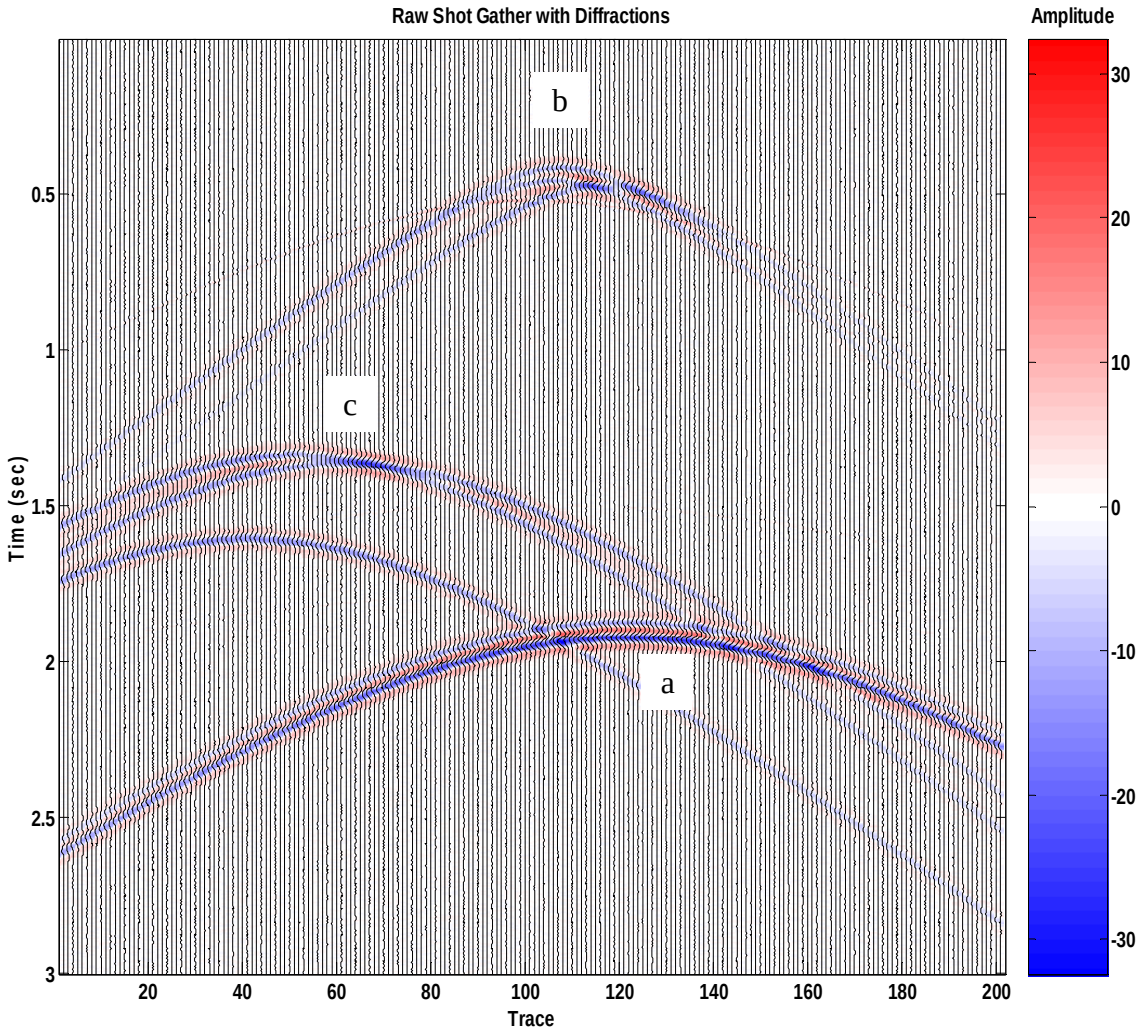

Figure 4-32: Synthetic shot gather from Line-2 of Model B.

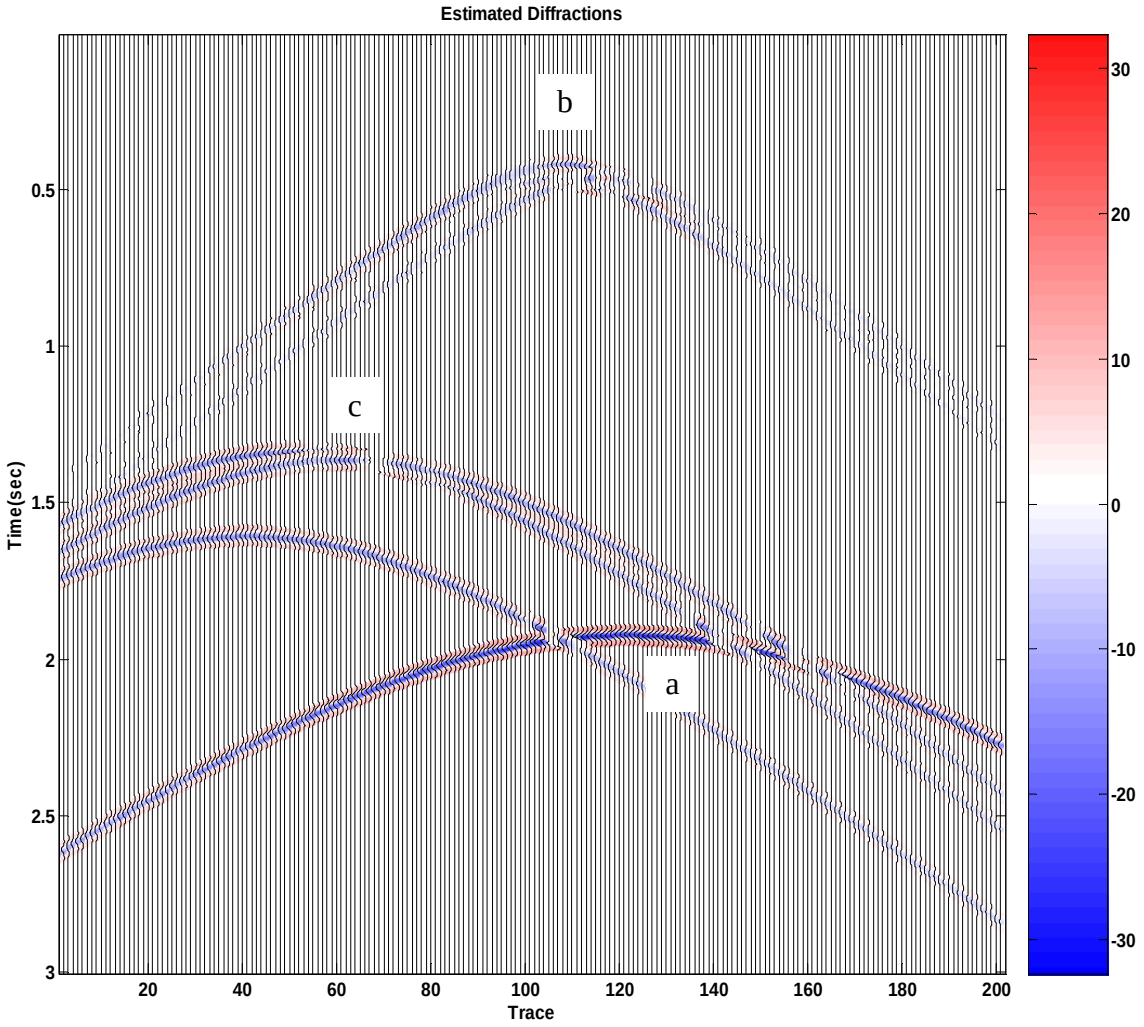

Figure 4- 33: Estimation of the three diffractions clusters from Line-2 of Model B.

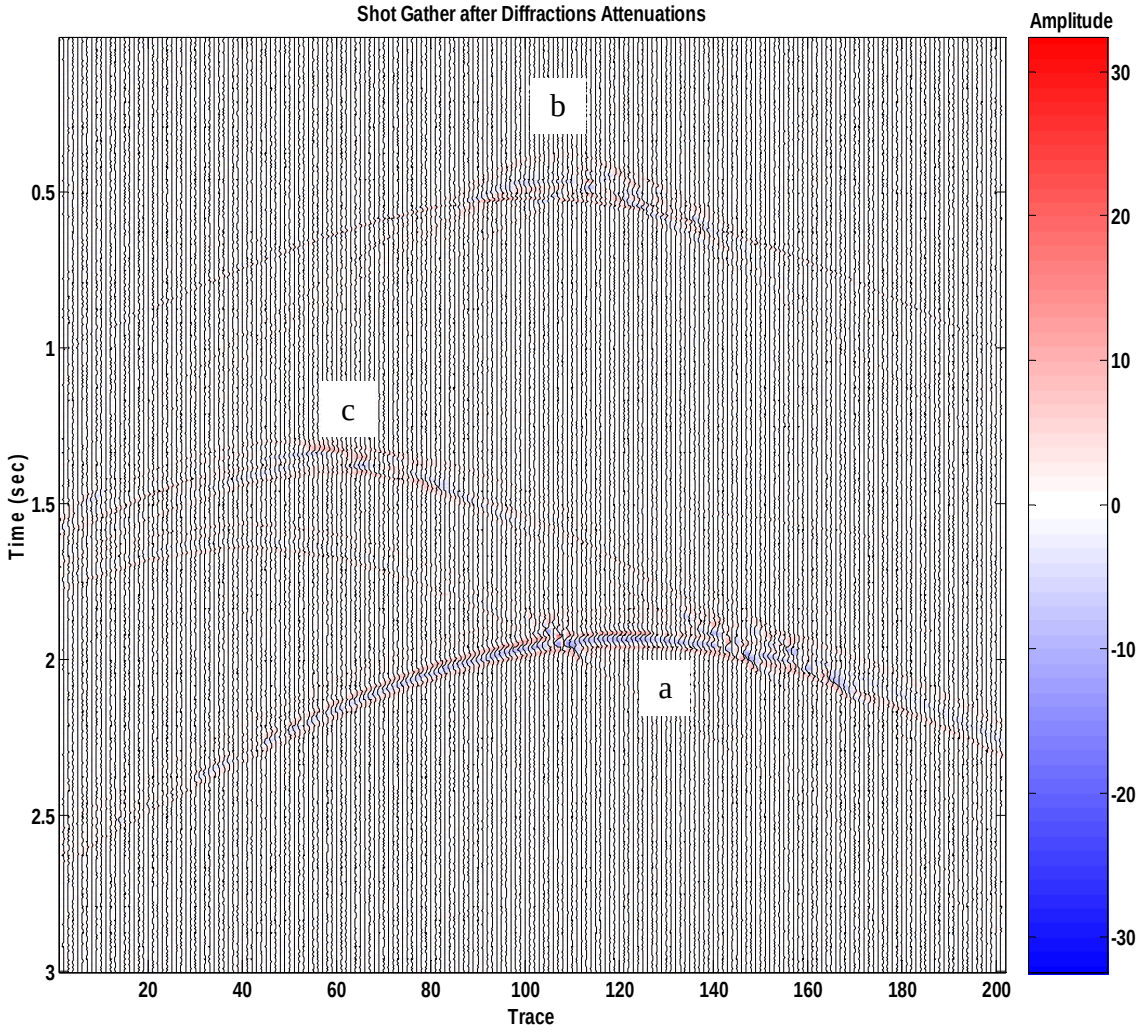

Figure 4- 34: Shot gather (Line-2 of Model B) after subtracting the estimated diffraction events.

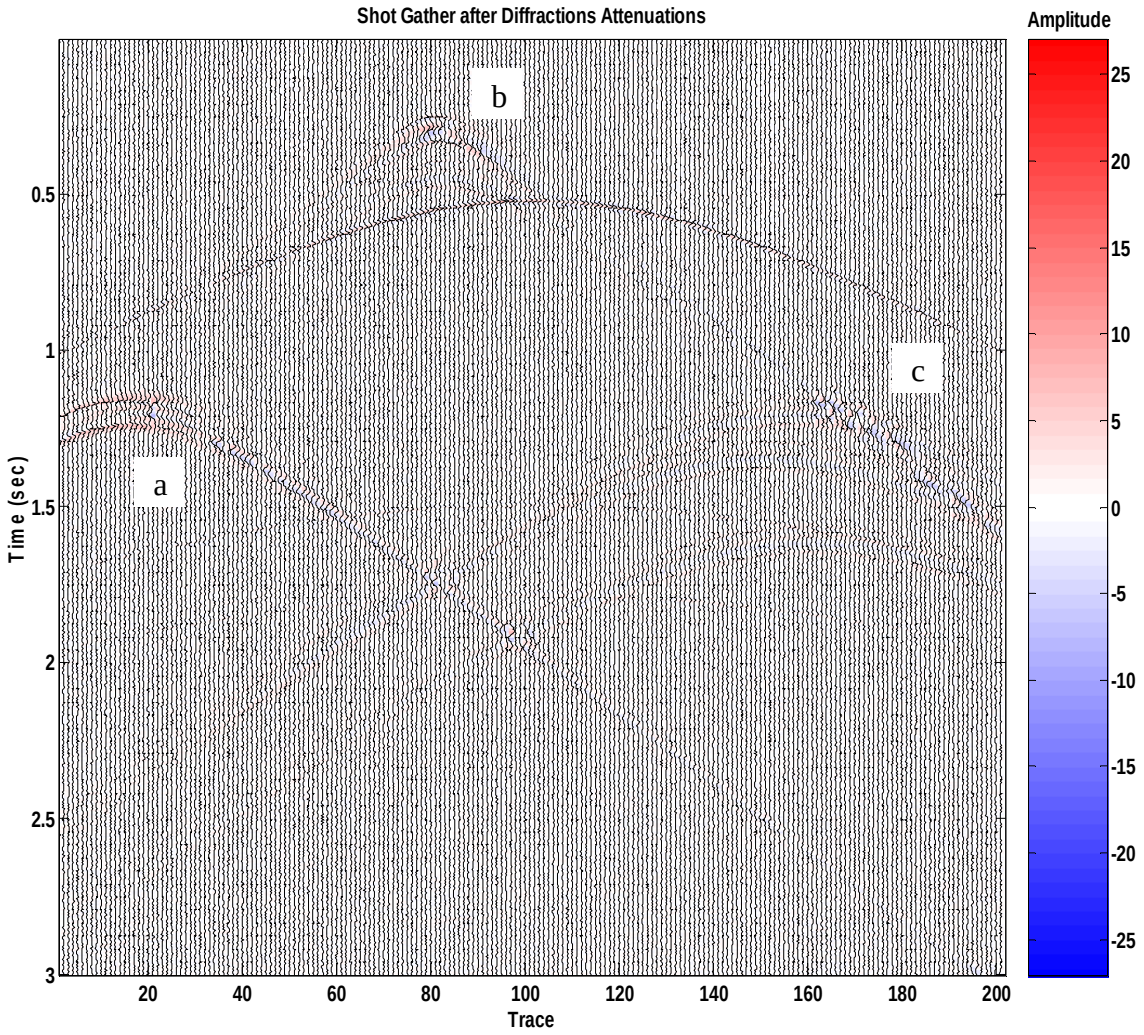

Figure 4- 35: Shot gather (Line-1 of Model B) after subtracting the estimated diffraction events using the true diffractor locations.

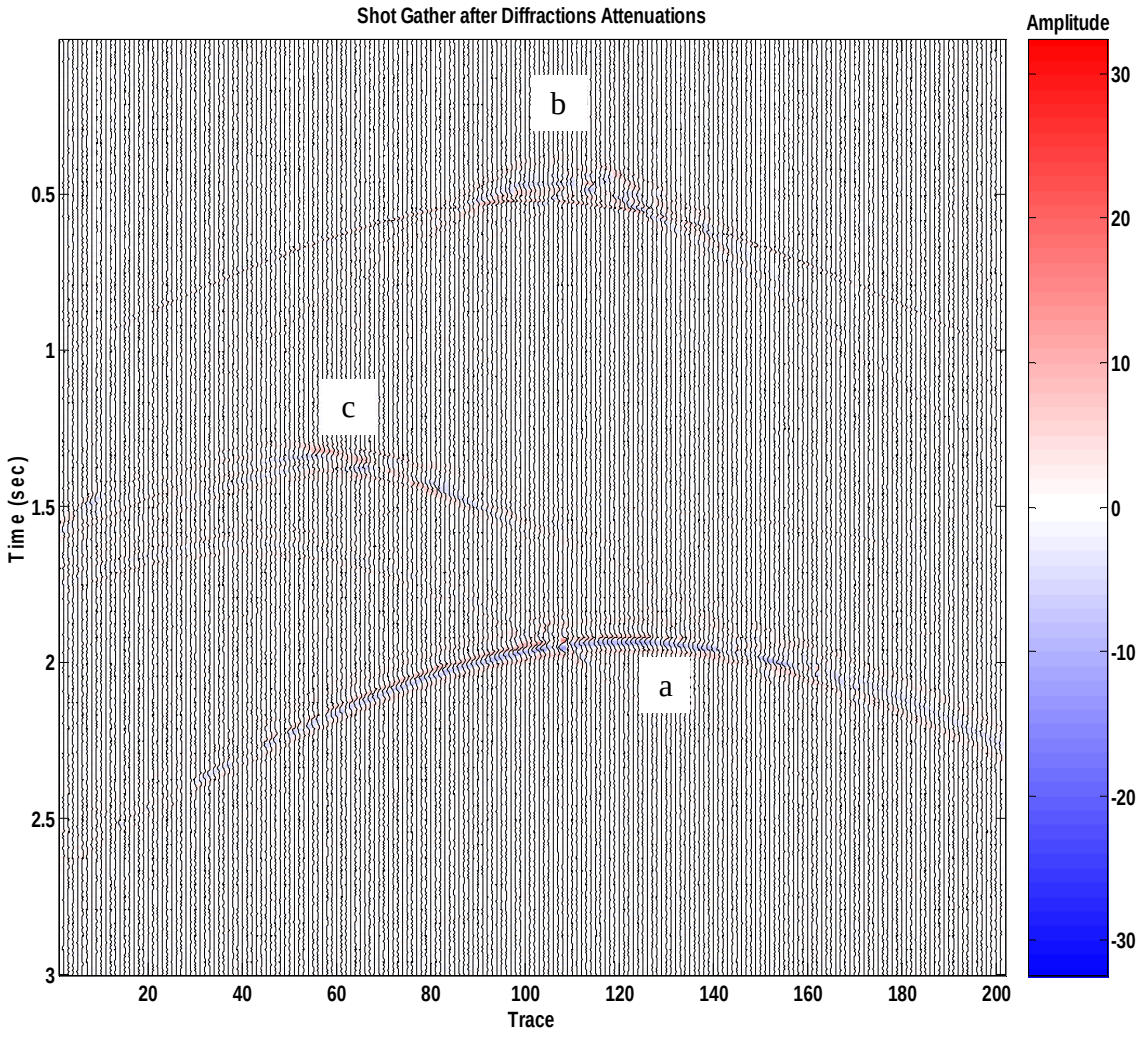

Figure 4- 36: Shot gather (Line-2 of Model B) after subtracting the estimated diffraction events using the true diffractor locations.

CHAPTER 5

CONCLUSIONS & RECOMMENDATIONS

5.1 Conclusions

Data driven processing algorithms to map near-surface diffractors of surface waves and attenuate their diffracted energy in seismic shot gathers were presented. The mapping algorithm is based on the time-offset (T-X) relation of side-scattered surface waves from near-surface diffractors and the semblance measurement. The attenuation algorithm employs least mean square estimation of the diffracted wavelet and subtracts it from the original data.

The algorithms have been applied successfully on synthetic data from two different models. In spite of the robustness of the algorithms when they were tested on synthetic data, tests on real data would be needed to confirm the strength of the method.

Although the algorithms are dealing with 2D shot gathers, the robustness of the method will be revealed even better when it is applied on 3D data. This is because we only need to extract few 2D lines from the 3D data scattered over the surveyed area and use the

mapping algorithm on those few lines to identify confidently the locations of the near-surface diffractors in the area. Then we use the attenuation algorithm to attenuate the mapped diffractors

5.2 Recommendations

Following are some recommendations and suggestions for more investigation and further development of the method:

1- To improve the attenuation of closely spaced diffractors whose energy are interfering on shot gathers, better estimation methods need to be investigated such as simultaneous estimation of the interfering diffractions.

2- The frequency of the diffracted surface wave is an important parameter in the algorithms, especially in attenuation and need to be carefully estimated.

3- To minimize the ambiguity of having mirror image maps, shot gathers with seismic source located within the line of receivers should be avoided if possible.

Bibliography

Al-Shuhail, A. A., and Al-Ghamdi, A. M., 2000, Removal of backscattered noise from shot records by forward modeling: Land Seismic Imaging Forum (Arabian Peninsula), Manama, Bahrain.

Blonk, B. and Herman, G. C., 1994, Inverse scattering of surface waves: A new look at surface consistency: Geophysics, 59, 963-972.

Baeten, G. J. M., Belougne, V., Combee, L., Kragh, E., Laake, A., Martin, J. E., Orban, J., Ozbek, A., and Vermeer, P. L. (2000) Acquisition and processing of point receiver measurements in land seismic: Ext. Abstr., 70th Ann. Internat. Mtg., SEG, 2000, 41-44.

Gulunay, N., Magesan, M., and Conner, J., 2006, Diffractor scan (DSCAN) for attenuating scattered energy: EAGE 68th Conference & Exhibition, Vienna, Austria, 12-15 June, 2006.

Herman, G. C., and Perkins, C., 2006, Predictive removal of scattered noise: Geophysics, 71, V41-V49.

Neidell, N. S., and Taner, M. T., 1971, Semblance and other coherency measurements for multichannel data: Geophysics, 36, 482-497.

Nemeth, T., Sun, H., and Schuster, G. T., 2000, Separation of signal and coherent noise by migration filtering: Geophysics, 65, 574-583.

Sayed, A., H., 2003, Fundamentals of Adaptive Filtering: John Wiley & Sons, Inc., Hobken, New Jersey.

Yilmaz, O., 1987, Seismic Data Processing: SEG. Tulsa, OK.

Vita

Ayman Fazea Al-Lehyani was born in Makkah, Saudi Arabia on January 23, 1978. In summer of 2002, he received a Bachelor of Science degree in Geophysics form King Fahd University of Petroleum and Minerals (KFUPM) with first honor. Directly after graduation Mr. Al-Lehyani joined Schlumberger Data and Consulting Services (DCS) in Dhahran, Saudi Arabia as a petrophysicist. He was part of a team that was devoted full-time to one of the biggest Saudi Aramco petrophysical projects. In February 2006, he joined the Geophysics Research Group at the newly established Schlumberger Dhahran Carbonate Research Center (SDCR) based in Dhahran Techno-Valley within the KFUPM Campus. He started his Master of Science in Geophysics at KFUPM in the fall semester of 2005. Mr. Al-Lehyani is a student member of the SEG and DGS.